

FUNCTIONALIZATION OF SINGLE-
WALLED CARBON NANOTUBES WITH
BIS-ASTRAPHLOXIN

EBRIMA SAHO
APPLIED PHYSICS BSc
2019

ASTON UNIVERSITY

© Ebrima Saho, 2019

Ebrima Saho asserts his moral right to be identified as the author of this thesis.

This copy of the thesis has been supplied on condition that anyone who consults it is understood to recognise that its copyright rests with its author and that no quotation from the thesis and no information derived from it may be published without appropriate permission or acknowledgement.

Summary

This dissertation aims to demonstrate that photoluminescence spectroscopy could be an efficient technique of functionalized carbon nanotube detection and imaging. The advances in nanotechnology and the potential growth in carbon nanotubes production, in which if control mechanisms not in place for safely disposing off nanotubes, these nanotubes could pose as an environmental pollutant, due to the severe, persistent and bio-accumulative nature of these compounds. Therefore, the need for this scientific research is timely in case of some technological disaster. Besides, the study on interaction of carbon nanotubes with various organic materials provide a new knowledge and opportunities for potential application of the nanotubes.

The dissertation starts by exploring and conducting an in-depth literature survey on the functionalization of carbon nanotubes, energy transfer and photoluminescence imaging and the project develops upon the previous work by P. Lutsyk et al. in *Light Sci Appl.* 5 (2016) e16028 entitled "*A Sensing Mechanism for the Detection of Carbon Nanotubes Using Selective Photoluminescent Probes Based on Ionic Complexes with Organic Dyes.*" The literature is followed by comprehensive experimental studies by optical spectroscopy techniques on a new system of carbon nanotubes with bis-astraphloxin, which is promising to provide a new insight into non-covalent functionalization of carbon nanotubes. The bis-astraphloxin is a new cyanine dye molecule consisting of two astraphloxin units linked together, where individual astraphloxin units have been studied before and showed strong energy transfer to the nanotubes.

The main findings from the experimental studies described in this dissertation illustrate that carbon nanotubes interact with bis-astraphloxin. This is evidenced by absorption spectra of the mixtures are not a superposition of the spectra of each component: the nanotubes or bis-astraphloxin dye only. In the studied mixtures of the nanotubes with bis-astraphloxin, we observe a strong quenching of visible range dye emission and significant enhancement (up to a factor of 4) of the near infrared emission of carbon nanotubes in the range of the dye excitation. This result is evidencing efficient energy transfer from the interacting donor, bis-astraphloxin, to acceptor, the nanotubes. Comparison of the bis-astraphloxin-nanotube mixture with the mixture of astraphloxin-nanotubes and relating to literature data, it is possible to associate the interaction and energy transfer due to the formation of ionic complexes of bis-astraphloxin-SWCNT. The compounds are self-assembled due to Coulomb attraction of positively charged bis-astraphloxin and positively charged nanotubes covered by negatively charged surfactant. Finally, it has been shown that higher concentration of bis-astraphloxin contribute to the formation of such complexes, which could be used for further design of functionalized carbon nanotubes.

Acknowledgments

I am very humbled and blessed to get involved in nanoscience research and now that this project has been completed. It equipped me with invaluable knowledge and expertise in the field of scientific research. Even though the project was highly demanding, I have gained all the necessary tools and skills. For example, it boosted my confidence in problem-solving, communication and I have progressed immensely in understanding empirical analysis of experimental data. It was a significant and exciting experience.

Therefore, I will begin to give thanks and praises to the Almighty God for providing me the strength to venture into this critical exploration.

I want to express my profound appreciation to my primary supervisor, Dr Petro Lutsyk who suggested this exciting research area and gave me all the necessary training before the start of the project. He supported and supervised me throughout this project. His valuable guidance and constant motivation have been the driving force that assisted me to remain focused on this project and mould it into full proof success. His recommendations and instructions were vital in the realization of the project.

Many thanks to my secondary supervisor Dr. Richard Martin for his initial suggestions and for aiding to ensure that my project remains on course.

Also, I would like to cordially thank Prof. Yu. Slominski and Dr. M. Shandura for the dye provision. Finally, I would like to thank my friends and my family for their tremendous support and advice especially in the last few weeks of this project.

Contents

SUMMARY	3
ACKNOWLEDGMENTS	5
LIST OF FIGURES	9
LIST OF TABLES	10
ABBREVIATIONS	11
1 INTRODUCTION	13
1.1 PRIMARY OBJECTIVES (PO) OF THE PROJECT	15
1.2 EXTENDED OBJECTIVE (EO) OF THE PROJECT	15
2 BACKGROUND	16
2.1 THE ALLOTROPES OF CARBON.....	16
2.2 CARBON NANOTUBES.....	18
2.2.1 <i>Types of Carbon Nanotubes and Related Structures</i>	18
2.2.2 <i>Single-Walled Carbon Nanotubes</i>	19
2.2.3 <i>Carbon Nanotubes Production</i>	19
2.2.4 <i>Functionalization of Carbon Nanotubes</i>	20
2.2.5 <i>Non-Covalent Functionalization of Carbon Nanotubes</i>	21
2.2.6 <i>Non-Covalent Interactions of CNTs with Surfactants and Ionic Liquids</i>	21
2.3 PURIFICATION OF CARBON NANOTUBES.....	22
2.4 MOLECULAR FLUORESCENCE.....	22
2.4.1 <i>Luminescence</i>	22
2.4.2 <i>Types of Luminescence</i>	23
2.4.3 <i>Luminescence Compounds</i>	23
2.4.4 <i>History of Fluorescence and Phosphorescence</i>	23
2.5 RESONANCE ENERGY TRANSFER.....	24
2.5.1 <i>Fluorescence Resonance Energy Transfer Process</i>	25
2.5.2 <i>Interactions Involved in Nonradiative Energy Transfer</i>	26
2.6 PHOTOLUMINESCENCE.....	27
2.6.1 <i>NIR Fluorescence of SWCNTs for Optical Sensing</i>	28
2.7 ULTRAVIOLET/VISIBLE/NEAR INFRARED (UV/VIS/NIR) SPECTROSCOPY	28
2.7.1 <i>Principles</i>	29
2.8 DYE – (ASTRAPHLOXIN).....	29
2.9 DYE - (BIS-ASTRAPHLOXIN)	30
2.10 SURFACTANT – (SDBS).....	31
3 PROCEDURE	32

Functionalization of single-walled carbon nanotubes with bis-astraphloxin

3.1	SAMPLE PREPARATION	32
3.1.1	<i>Sample Cell</i>	33
3.1.2	<i>SWCNT Sample Preparation</i>	33
3.1.3	<i>A mixture of Initial SWCNT with Organic Dye</i>	33
3.2	ABSORPTION CHARACTERIZATION EXPERIMENTAL SETUP.....	34
3.3	PHOTOLUMINESCENCE (PL) CHARACTERIZATION EXPERIMENTAL SETUP.....	36
4	EXPERIMENTS	38
4.1	MEASURING ABSORPTION	38
4.1.1	<i>Zero-line calibration of the spectrometer</i>	39
4.1.2	<i>Immediate Measurements of Absorption</i>	39
4.1.3	<i>Delayed or Temporal Measurements of Absorption</i>	39
4.2	RESULTS	40
4.2.1	<i>Immediate Measurement of Dye and CNT</i>	40
4.2.2	<i>Immediate Measurement of the Mixtures</i>	41
4.2.3	<i>Delayed/Temporal Measurement Results</i>	42
4.3	DISCUSSION/ANALYSIS.....	43
4.4	MEASURING FLUORESCENCE EMISSION/ MAPS	45
4.4.1	<i>Fluorescence Spectrometer System Calibration</i>	45
4.4.2	<i>Immediate measurement of Samples in VIS/NIR</i>	45
4.5	RESULTS	47
4.5.1	<i>Immediate Measurement of PLE Maps of Bis-astraphloxin and Astraphloxin</i>	47
4.5.2	<i>Neat CNT and A Mixture of CNT with Bis-astraphloxin</i>	48
4.5.3	<i>Mixtures of CNT with Dyes</i>	50
4.5.4	<i>PL Spectra of Neat CNT and the Mixtures</i>	51
4.5.1	<i>A Mixture of CNT with Bis-astraphloxin Measured Fresh and Measured After a Week</i>	52
4.6	DISCUSSIONS/ANALYSIS.....	53
4.7	GENERAL CHALLENGES AND MITIGATION	55
5	CONCLUSION	56
6	REFERENCES	58
7	APPENDIX- MAPS	60

List of Figures

FIGURE 1: NEW SYSTEM.....	14
FIGURE 2: REFERENCE SYSTEM.....	14
FIGURE 3: THE PERIODIC TABLE INDICATING CARBON.....	17
FIGURE 4: THE GENERATION OF SYNTHETIC CARBON ALLOTROPES	17
FIGURE 5: FULLERENE C ₆₀ MODEL AND SINGLE-WALLED CARBON NANOTUBES (SWCNT)	18
FIGURE 6: SINGLE-WALLED CARBON NANOTUBES FORMED FROM 2-DIMENSIONAL FULLERENE	19
FIGURE 7: DIFFERENT ROUTES FOR NANOTUBES FUNCTIONALIZATION	20
FIGURE 8: ILLUSTRATION OF THE FLUORESCENCE RESONANCE ENERGY TRANSFER (FRET) PROCESS..	25
FIGURE 9: TYPES OF INTERACTIONS INVOLVED IN THE NONRADIATIVE TRANSFER MECHAN..	27
FIGURE 10: BIS-ASTRAPHLOXIN DOUBLE MOLECULE DIAGRAM.....	29
FIGURE 11: MOLECULAR STRUCTURE OF ASTRAPHLOXIN	30
FIGURE 12: PHOTO OF THE PERKIN ELMER 1050 SPECTROMETER.....	30
FIGURE 13: SCHEMATIC SETUP OF THE PERKIN ELMER SPECTROMETER	34
FIGURE 14: FLUORESCENCE SPECTROMETER.....	35
FIGURE 15: FLUOROLOG-3 SPECTROMETER	36
FIGURE 16: PREPARED SAMPLES.....	36
FIGURE 17: ADDITION OF SURFACTANT TO CNT AND MIXTURE OF CNT-SURFACTANT-DYE	38
FIGURE 18: ABSORPTION SPECTRA OF BIS-ASTRAPHLOXIN, CNT, DILUTED CNT, CNT-BIS-ASTRA ...	40-41
FIGURE 19: ABSORPTION SPECTRA OF BIS-ASTRAPHLOXIN, ASTRAPHLOXIN, SWCNTs-SDBS.....	41-42
FIGURE 20: ABSORPTION SPECTRA OF MIXTURE OF DIFFERENT CONCENTRATIONS.....	43
FIGURE 21: VISIBLE RANGE DYE EMISSION BEFORE MIXING	47
FIGURE 22: PHOTOLUMINESCENCE EXCITATION (PLE) MAPS FOR WATER SOLUTIONS	48-49
FIGURE 23: A MIXTURE OF CNTs WITH DYE.....	50
FIGURE 24: DEPENDENCE OF PL ON ORGANIC DYE CONCENTRATION IN THE MIXTURE OF CNT-SDBS	51
FIGURE 25: A COMBINATION OF CNT WITH NEW ORGANIC DYE	52

List of Tables

TABLE 1: VARIOUS TYPES OF LUMINESCENCE	23
TABLE 2: ELECTROMAGNETIC RADIATION WAVELENGTHS.....	29
TABLE 3: DIFFERENT SAMPLE MIXTURES AND VOLUME MEASUREMENTS.....	34
TABLE 4: SETTINGS FOR MEASUREMENTS IN VISIBLE RANGE	46
TABLE 5: SETTINGS FOR MEASUREMENTS IN INFRARED RANGE.....	46

Abbreviations

SWCNT/CNT	Single-walled-carbon nanotubes/ Carbon nanotubes
DWCNT	Double-walled-carbon nanotubes
MWCNT	Multi-walled-carbon nanotubes
NIR	Near infrared
VIS	Visible
UV	Ultraviolet
PO	Primary objective
EO	Extended objective
SDS	Sodium dodecyl sulphate
SDBS	Sodium dodecylbenzene sulfonate
AFM	Atomic force microscopy
RET	Resonance energy transfer
FRET	Förster resonance energy transfer
QY	Quantum yield
T	Transmittance
CBM	Common beam mask
InGaAs	Indium gallium arsenide phosphide
λ_{\max}	absorbance maximum
D	donor
A	acceptor
D/A	donor-acceptor
λ_{EX} or EX wavelength	excitation wavelength
λ_{EM} or EM wavelength	emission wavelength
PL	photoluminescence
PLE map	PL excitation-emission maps

1 Introduction

The discovery of carbon nanotubes captured the attention of researchers due to their combination of desirable intrinsic properties such as high tensile strength, elasticity, electrical and thermal conductivity. The research effort continues due to their excellent configurability and broad scope for modification giving many avenues for investigation and application.

Of special interest are 1-dimensional single-walled carbon nanotubes (SWCNTs) formed by rolling 2-dimensional graphene. This structure benefits from intrinsic near-infrared (NIR) fluorescence (900-1400 nm), which overlaps the spectral region in which biological tissues are optically transparent. Functionalized nanotubes are then ideal for highly targeted detection, monitoring, and therapy of diseases [1]. However, as nanotubes are resilient to natural processes of degradation, they can endure in the environment for long periods of time thus posing a problem as a pollutant potentially disrupting the ecosystem. For this reason, an efficient method for nanotube detection is required.

This project started in September 2018 and ended in May 2019. The project develops upon the work by P. Lutsyk et al. [2] and aims to demonstrate that photoluminescence spectroscopy could be an efficient technique of carbon nanotube detection and imaging. Current issues which this project seeks to address includes:

- The enhancement of photoluminescence from SWCNTs via energy transfer from organic dyes.
- The stability of non-covalently interacting SWCNT-dye systems not fully explored.

Of particular interest are the physical mechanisms for the interaction of carbon nanotubes with the previously non-investigated organic dye, bis-astraphloxin, which is supposed to yield significant amplification of photoluminescence response via resonant energy transfer. The project was initially launched to address the problems via the study of a novel SWCNT-dye system with energy transfer and exploration of a new organic dye, bis-astraphloxin. Bis-astraphloxin is a new cyanine dye molecule consisting of two astraphloxin units linked together forming a modified analogue of astraphloxin that showed a significant enhancement of photoluminescence via energy transfer [2]. In early November 2018 after the project plan and proposal was presented to the secondary supervisor Dr. Richard Martin. The suggestion was that it would be necessary if astraphloxin is also included in the investigation to compare and use it as a reference system. The difference between the two systems is the type of dye used. The new system uses a novel organic dye called bis-astraphloxin as in Figure 1, while the reference system uses simple analogue astraphloxin as in Figure 2.

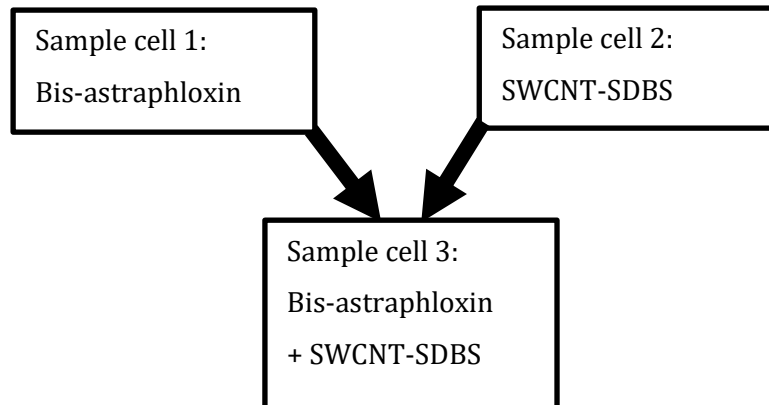


Figure 1 - New system

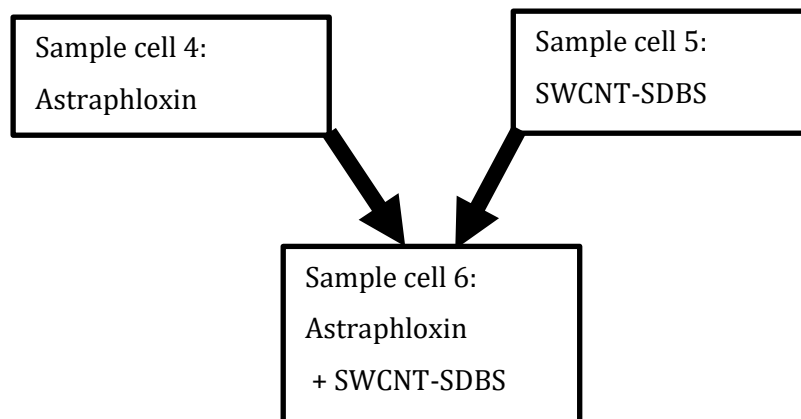


Figure 2 - Reference system

This dissertation will focus on the uninvestigated dye called bis-astraphloxin and will briefly look into the previously studied dye named astraphloxin for comparison reasons and to aid in concluding which dye is better at enhancing photoluminescence through resonance energy transfer based on the following primary and extended objectives: -

Primary Objectives:

- Literature review on SWCNT functionalization, energy transfer, and photoluminescence imaging.
- Experiments with mixtures of SWCNTs and bis-astraphloxin to explore energy transfer and enhancement of photoluminescent signal.
- An empirical analysis of experimental data, to develop the mechanism of interaction of bis-astraphloxin with SWCNTs.

Extended Objectives:

- Experiments and analysis of temporal evolution of energy transfer or aggregation in the SWCNT-dye mixtures.

Therefore, for the successful completion of this project, different milestones and deliverables dates were set from September 2018 to May 2019. The following primary and extended objectives show the individual landmark and deliverable end dates.

1.1 Primary Objectives (PO) of the Project

PO1 - Literature Survey on SWCNT Functionalization, Energy Transfer and Photoluminescence Imaging

Milestone M1.1 - Preliminary literature review (completed by 15th of October 2018)

Deliverable D1.1 - Literature review as a chapter for the dissertation (completed by 14th of December 2018).

PO2 - Experiment for Mixtures of SWCNT with Bis-Astraphloxin

Milestone M2.1 - Preliminary training on experimental measurements of absorption and photoluminescence spectra, including excitation-emission photoluminescence maps (completed by 25th of January 2019).

Milestone M2.2 - Samples preparation: neat dispersion of SWCNT, neat solution of the dye, and mixtures of the SWCNT with bis-astraphloxin (completed by 18th of February 2019).

Deliverable D2.1 - Measurements of absorption and photoluminescence spectra for the samples (completed by 18th of February 2019).

PO3 - Empirical Analysis of Experimental Data

Deliverable D3.1 - Physical mechanism proposed for the energy transfer in the SWCNT-dye system (completed by 22nd of February 2019).

1.2 Extended Objective (EO) of the Project

E04 - Experiment and Analysis of Temporal Developments of Energy Transfer/Aggregation in the SWCNT-Dye Mixtures

Deliverable D4.1 - Temporal measurements of absorption and photoluminescence spectra for the samples (completed by 11th of March 2019).

Deliverable D4.2 - An updated physical mechanism for the SWCNT-dye energy transfer (completed by 22nd of March 2019)

For the purpose of data acquisition and for effective empirical data analysis, OriginLab was selected because of the various in-built tools for linear, polynomial and nonlinear curve and surface fitting. It also provides several features for peak analysis, which is very helpful throughout the course of this project.

2 Background

The inspiration for this project is the extension upon the advances in functionalization of carbon nanotubes and its practical applications in reinforcement composites, biomedicine, sensors, and energy generation/transport/storage [1-3]. For example, unique electrical, thermal and spectral properties of carbon nanotubes functionalized by organic molecules offer further biomedical advances in the detection, monitoring, and therapy of diseases because the cells can comfortably internalize the functionalized carbon nanotubes and consequently acts as a transportation vehicle for different molecules applicable to treatment and diagnosis [3,4].

The energy transfer from the organic molecules to SWCNTs enables robust sensitization of photoluminescent response from the nanotubes and this way the SWCNTs detected in the natural environment in case of some technological disaster [2]. The literature review of SWCNT functionalization, energy transfer, and photoluminescence imaging cover 10 main topics which this dissertation explored. Mentioned below are the subjects discretely highlighted.

- The Allotropes Carbon
- Carbon nanotubes
- Purification of carbon nanotubes
- Molecular fluorescence
- Resonance energy transfer
- Photoluminescence imaging
- UV/VIS/NIR Spectroscopy
- Dye (bis-astraphloxin)
- Dye (astraphloxin)
- Surfactant (SDBS)

This literature review studied each basic theme concepts and practical applications. Therefore, the following chapter will discuss the literature survey on the following topics above in detail.

2.1 The Allotropes of Carbon

Carbon is an element with atomic number 6 that can be found on the periodic table (see Figure 3). It provides the basis for life on earth. Elemental carbon has many technological applications, ranging from drugs to synthetic materials. Due to the structure and electronic configuration of Carbon, it can bind to itself and practically to most of the other elements in an endless variety. The resulting structural diversity of organic compounds and molecules accompanied by a broad range of chemical and physical properties [4].

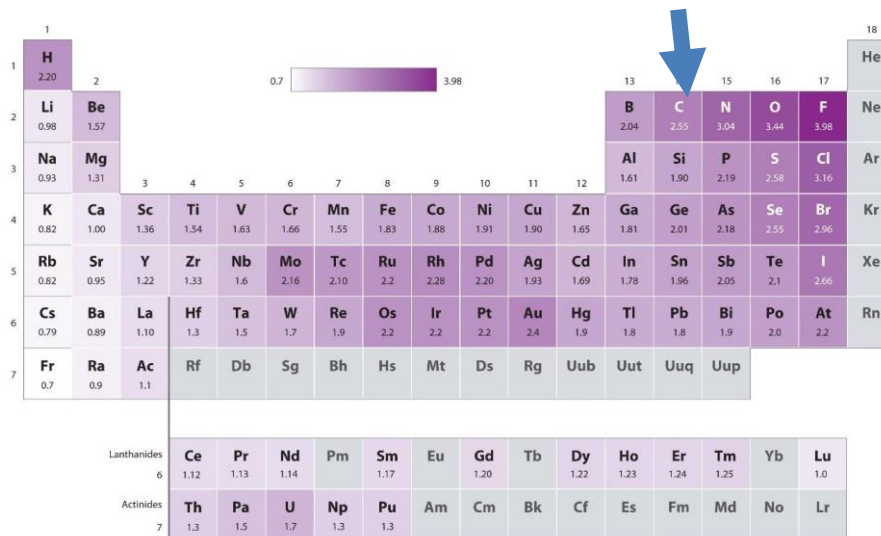


Figure 3: The periodic table indicating carbon [5].

The principal carbon as shown in the periodic table exists in two natural allotropes, diamond, and graphite, which consist of extended networks of sp^3 - and sp^2 -hybridized carbon atoms, respectively. These natural allotropes indicated distinctive physical properties such as hardness, thermal conductivity, lubrication behaviour or electrical conductivity. The allotropes can be constructed in many ways by altering the periodic binding shape in networks consisting of sp^3 -, sp^2 - and sp -hybridized carbon atoms [4].

The two known allotropes of carbon existed for a while before the discovery of fullerene in 1985, carbon nanotubes in 1991, and graphene in 2004 as shown in Figure 4. The observations marked the beginning of an *era of synthetic carbon allotropes*. The countless possible ways of alterations and number of scientists probing this challenge, guarantee that the revelations and discoveries in this area will continue [4].

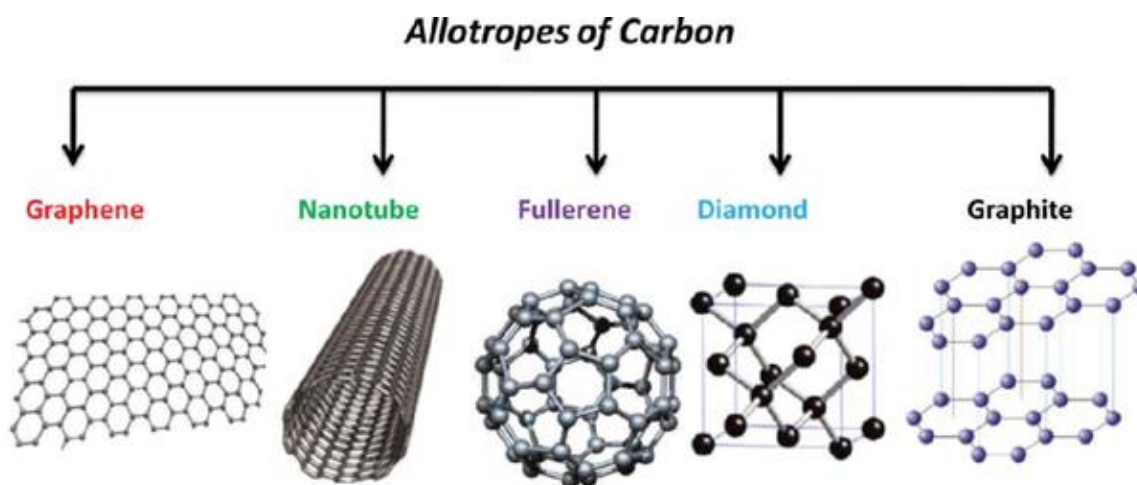


Figure 4: The generation of synthetic carbon allotropes [6].

2.2 Carbon Nanotubes

The discovery of a spherical molecule composed exclusively of carbon atoms as in Figure 5 was uncovered in 1996 by three great scientist namely Harry Kroto, Robert Curl, and Richard Smalley. These scientists were awarded a Nobel prize in Chemistry for such a phenomenal revelation [7].

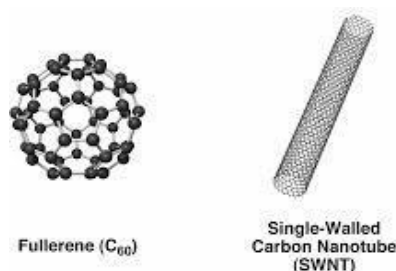


Figure 5: Fullerene C₆₀ model on the left [8]. Fullerenes are close cage clusters relatively stable in the gas phase [7]. The single-walled carbon nanotubes on the right are elongated structures that can reach several microns in length and small diameter in the nanometer range.

The nanometre-scale framework was named “fullerene” because of its resemblance to the extremely conformity architectonic geodesic domes designed by the architect Richard Buckminster Fuller. Extensive studies were carried out in the 1980s and the early 1990s on fullerene theory, synthesis, and its characterization. In 1991 Lijima, presented transmission electron microscopy observations of elongated and concentric layered microtubules made of carbon atoms, which considered as filamentous carbon. The surveillance by Lijima, catapulted the substantial investigations corresponding to one of the most actively studied shapes of the last century, presently named carbon nanotubes (CNTs) [7].

2.2.1 Types of Carbon Nanotubes and Related Structures

There are different types of carbon nanotubes, which are given below. The focus here is the single-walled carbon nanotubes, and other types of carbon nanotubes not discussed in this review.

- Single-walled carbon nanotubes (SWCNTs)
- Multi-walled carbon nanotubes (MWCNTs)
- Double -walled carbon nanotubes (DWCNTs)
- Junctions and Crosslinking
- Other morphologies
- Extreme carbon nanotubes

2.2.2 Single-Walled Carbon Nanotubes

The shape and structure of carbon nanotubes conceptualized as a rolled-up sheet of graphene (Figure 6), which is a planar – hexagonal arrangement of carbon atoms distributed in a honeycomb lattice [7].

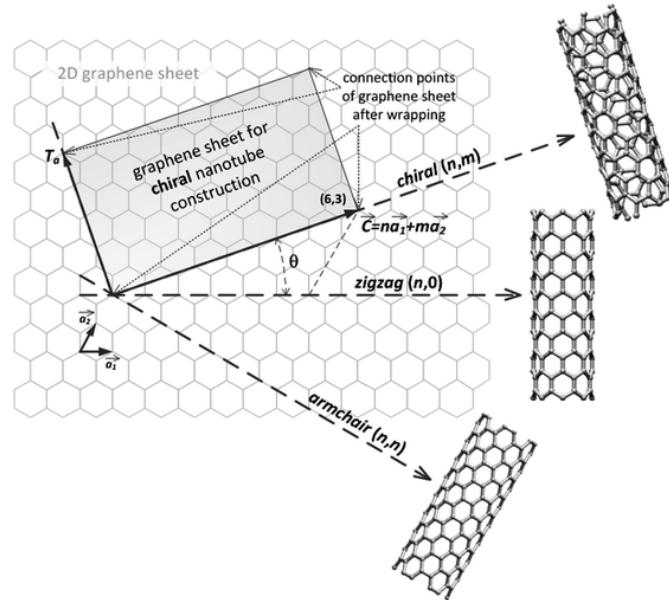


Figure 6: A single-walled carbon nanotubes formed from 2-dimensional graphene [9].

From Figure 6 we can see that the nanotubes are classified into three main categories according to the rolling direction, namely, zigzag, armchair, and chiral. From an underlying perspective and for future practical applications the most prominent characteristics of SWCNT are that they exhibit unique electronic (semiconducting or metallic), mechanical (Young Modulus), optical and chemical characteristics [4].

2.2.3 Carbon Nanotubes Production

There are different methods for producing SWCNT as indicated below. Each of the production techniques has an associated advantage as well as disadvantage. The most established high-temperature techniques are arc discharge and laser ablation, as well as chemical vapour deposition (CVD) with its common variants [4]. The literature regarding the synthesis of SWCNTs is inexhaustible, but far from being fully understood.

- Arc discharge
- Laser ablation
- Chemical vapour deposition
- Miscellaneous synthesis methods

The state-of-the-art carbon nanotubes production entails many approaches and new paths continuously evolved.

2.2.4 Functionalization of Carbon Nanotubes

Functionalization of carbon nanotubes have two broad categories (see Figure 7)

- covalent functionalization
- non-covalent functionalization

The idea of functionalizing carbon nanotubes implemented because of the outer wall of the pristine nanotubes being resistant and conceived as chemically inert. The inactive behaviour of these nanotubes is not consistently advantageous for applications and this ground, modifying the properties of carbon nanotubes in a controlled manner have been thought of to make them chemically active. The process of chemically activating can be implemented using one of the several functionalization routes convenient. It is crucial revealing that in many cases the term functionalization could be too broad to explain the kind of changes desired. The concept means in-lattice doping, intercalation, molecule or particle adsorption, encapsulation, or even other nonexposed modifications [4].

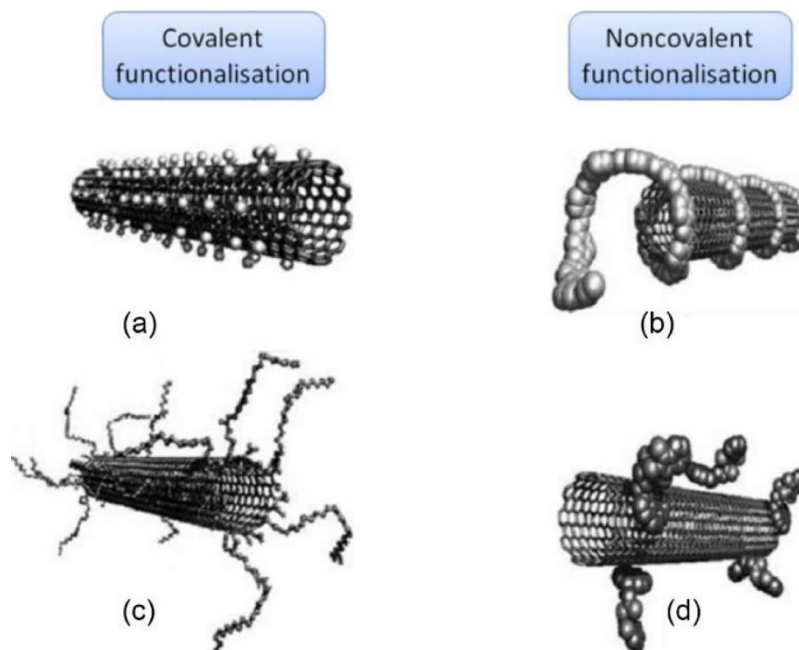


Figure 7: Different routes for nanotubes functionalization: (a) sidewall covalent functionalization, (b) defect-group covalent functionalization, (c) Non-covalent polymer wrapping, (d) Non-covalent pi-stacking.

The centre of attention in the next subsection will be non-covalent functionalization of carbon nanotubes, which is the focal point in this research. This survey will not explore the covalent functionalization of carbon nanotubes.

2.2.5 Non-Covalent Functionalization of Carbon Nanotubes

CNTs manifested unique mechanical, optical and electrical properties that model them perfect nanoscale materials. Notwithstanding, the suggested application mentioned above limited by their experimental insolubility in aqueous and organic solvents. Due to the high polarizability and smooth surface of carbon nanotubes, and, SWCNTs in particular – form bundles and ropes, whereby individual nanotubes are positioned parallel to each other with Van der Waals attraction. Also, CNTs obtained as mixtures that demonstrated different chiralities, diameter, and length, in which non-carbon nanotubes and metal catalysts are also present in the final material [7].

Some of these hindrances overpowered by the controlled defect and sidewall functionalization of CNTs. The formation of covalent linkages can drastically enhance the solubility of CNTs in various solvents while guarantees the structural integrity of the nanotube skeleton, but it also alters the intrinsic physical properties of the CNTs due to the modification of the sp² carbon framework. The most important effect is that the inherent conductivity of the CNTs destroyed. [7]

A possible and alternative strategy for preserving the unique electronic and mechanical properties of CNTs is by non-covalent or supramolecular modifications of CNTs. Non-covalent interactions entail hydrophobic, van der Waals, and electrostatic forces, and require the physical adsorption of suitable molecules onto the sidewalls of the CNTs. Non-covalent functionalization is achieved by polymer wrapping, adsorption of surfactants or small aromatic molecules, and interaction with porphyrins or biomolecules such as DNA and peptides [7].

2.2.6 Non-Covalent Interactions of CNTs with Surfactants and Ionic Liquids

Significant progress towards the solubilization of CNTs in water, which is crucial because of potential biomedical applications and biophysical processing schemes, has been achieved by using surfactants. Among the surfactants, the anionic surfactant sodium dodecyl sulphate (SDS) has been the most widely used surfactant [7].

Surfactant molecules containing aromatic groups can form more specific and more direction π - π stacking interactions with the graphite surface of CNTs. Interactions of SDS and the structurally related sodium dodecylbenzene sulfonate (SDBS) with SWCNTs have been compared to indicate the role of the aromatic rings. SDS and SDBS have the same length of the alkyl chain, but the latter has a phenyl ring attached between the alkyl chain and the hydrophilic group. The presence of the phenyl ring makes SDBS more effective for solubilization of CNTs than SDS, because of the aromatic stacking formed between the SWCNTs and the phenyl rings of the SDBS within the micelle. The diameter distribution of CNTs in the dispersion of SDBS,

measured by atomic force microscopy (AFM), showed that even at 20mg/ml $\sim 63 \pm 5\%$ of the SWCNT bundles exfoliate in single tubes [7].

2.3 Purification of Carbon Nanotubes

CNT material decontaminated due to the different procedures of production employed. The methods of synthesis utilized vary from each other, and the presence of unwanted by-products in the soot is unavoidable. These contaminants interfere with the exceptional properties of the nanotubes. The method of determining the degree of nanotubes purity is debatable because there is no consolidated standard to follow based on the reference uses of synthesized materials. Several methods used in SWCNT purification and none of the mechanisms is ubiquitous. The cleaning employs different oxidation steps, and the main processes given below.

- Sonication
- Thermal treatments
- Chemical acid treatments
- Others

It is very paramount to understand even after the processes mentioned above; nanotubes still need to be separated because of the existence of a different number of walls in the mixture of the nanotubes. There are 2 well known possible separation techniques of nanotubes called electrophori-based and ultracentrifugation-based. However, the idea of purifying a nanotube is still questionable due to the number of parameters that could be considered [7].

2.4 Molecular Fluorescence

2.4.1 Luminescence

The spontaneous emission of radiation from an electronically or vibrationally excited species that are not in thermal equilibrium with its environment [10]. Light emission classified into nine different types, and this grouping based on the mode of excitation. Table 1 gives the various types of fluorescence.

2.4.2 Types of Luminescence

Table 1: Various types of luminescence [13].

Phenomenon	Mode of excitation
Photoluminescence (fluorescence, phosphorescence, delayed fluorescence)	Absorption of light (photons)
Radioluminescence	Ionizing radiation (α , β , γ)
Cathodoluminescence	Cathode rays (electron beam)
Electroluminescence	Electric field
Thermoluminescence	Heating after prior storage of energy (e.g., radioactive irradiation)
Chemiluminescence	Chemical reaction (e.g. oxidation)
Bioluminescence	In vivo biochemical reaction
Triboluminescence	Frictional and Electrostatic forces
Sonoluminescence	Ultrasound

2.4.3 Luminescence Compounds

There are three different types of luminescent compounds

- Organic compounds (aromatic hydrocarbons and derivatives, dyes, etc.)
- Inorganic compounds (doped glasses, semiconductor nanocrystals, metal clusters, carbon nanotubes, and some fullerenes, etc.)
- Organometallic compounds (porphyrin metal complexes, ruthenium complexes, copper complexes, etc.)

Importantly, photoluminescence can be divided into two significant classes called fluorescence or phosphorescence and it is the concept of light absorption by matter, and the absorbing species elevated to an electronically excited state. The spontaneous emission of photons accompanying de-excitation is term as photoluminescence, which is the possible effects resulting from the interaction of light with matter [10]. Stimulated emission is also possible under certain conditions.

2.4.4 History of Fluorescence and Phosphorescence

The term phosphorescence comes from 2 Greek words. The first one being 'φωG' meaning light or photon and the second one 'φοπεlv' meaning to bear. Therefore, phosphor means something

that takes light and is the term assigned to materials that carry glow in the dark after being exposed to light since the middle ages [10].

On the other hand, fluorescence is not that obvious. The idea came from a phenomenal physicist and a professor of mathematics Sir George Gabriel Stokes of Cambridge University in the middle of the 19th century. But the primary purpose of fluorescence came from a Spanish physician, Nicolas Monardes, in 1565. He initially observed the incredible blue colour of an infusion of a wood brought from Mexico used to treat Kidney and urinary diseases [10].

2.5 Resonance Energy Transfer

The initial consideration of the nonradiative transfer of excitation energy – also called resonance energy transfer (RET) - from a new species to another one was outlined with atoms in the gas phase. G. Cario and J. Franck indicated in 1922 that upon selective excitation of mercury atoms at 254nm in a vapor mixture with thallium atoms, sensitized emission of the latter can be detected at 535nm. H. Kallman and F. London developed a quantum theory of resonance energy transfer via dipole-dipole interaction in the gas phase in 1928. The concept of the critical radius (distance at which transfer, and natural decay of the excited donor are equally probable) was introduced [10].

In solutions, when increasing the concentration of fluorescence in a viscous solvent, E. Gaviola and P. Pringsheim observed in 1924 that the fluorescence polarization gradually decreases but did not explain the result. It was only in 1929 that Francis Perrin correctly explained it because of homo-transfer. Years before, in 1925, his father Jean Perrin proposed the mechanism of resonance energy transfer. F. Perrin developed in 1932 a quantum mechanical theory of homo-transfer and qualitatively discussed the effect of spectral overlap [10].

A crucial milestone in the chronicle of fluorescence was when Theodor Förster around 1946 developed the complete theory of resonance energy transfer via dipole-dipole interaction and based on the idea of both classical and quantum mechanical approaches.

Instead of resonance energy transfer, the word fluorescence resonance energy transfer was introduced and initially emerged in life science papers. The confusion is because fluorescence does not transition resonance energy transfer, which is a nonradiative process. To avoid the misnomer, it is crucial to consider the F in FRET to stand for Förster or Förster-type instead of fluorescence. Notwithstanding, resonance energy transfer is not just limited to Förster-type transmission, that is, via dipole-dipole interaction.

In the late 1970s and early 1980s, (F) RET has been used as a spectroscopic ruler. It is ideal for measuring the distance between a donor chromophore and an acceptor chromophore in the range of 1 – 10 nm, which used in monitoring or separation of two species [10].

2.5.1 Fluorescence Resonance Energy Transfer Process

FRET is a non-radiative procedure whereby a donor (usually a fluorophore) upon excitation goes into an excited state. The excited state transfers energy to a proximal ground state acceptor A through long-range dipole-dipole interactions as in Figure 8. The acceptor absorbs light at the emission wavelength of the donor and does not always have to transmit the light fluorescently (i.e., dark quenching). The rate at which energy transfer occurs mainly depends on factors such as spectral overlap, the relative orientation of the transition dipoles and the distance r between donor and acceptor molecules.

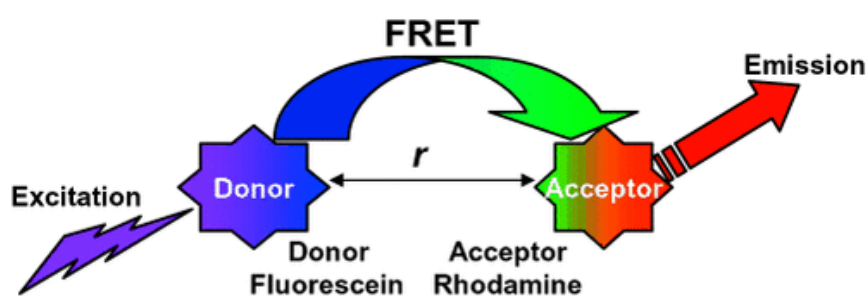


Figure 8: Schematic illustration of the FRET process: when the donor is excited, the excited molecule transfer energy to the acceptor molecule non-radiatively. A distance r separates the donor and acceptor. The acceptor molecule can release energy either radiatively or non-radiatively [10].

FRET usually occurs over distances comparable to the dimensions of most biological macromolecules, that is, about 10 to 100 Å. However, formations in which several donors and acceptors interact are progressively typical. The following equations evaluate energy transfer between a single linked D/A pair separated by a fixed distance r which comes from the theoretical treatment of Foster. The energy transfer rate $K_T(r)$ between a single D/A pair is dependent on the distance between D and A and can be expressed in terms of the Förster distance R_0 . R_0 is the distance between D and A at which 50% of the excited D molecules decay by energy transfer, while the other half decay through other radiative or non-radiative channels. R_0 can be calculated from the spectral properties of the D and A species as in equation 1 [11].

$$R_0 = 9.78 \times 10^3 [K^2 n^{-4} Q_D J(\lambda)]^{\frac{1}{6}} (\text{Å}) \dots \dots \dots \text{(Equation 1)}$$

The factor K^2 describes the D/A transition dipole orientation and can range in value 0 (perpendicular) to 4 (collinear/parallel). The controversy about which dipole orientation to assign to a specific FRET format is huge. Only in few cases can the crystal structure of the D/A

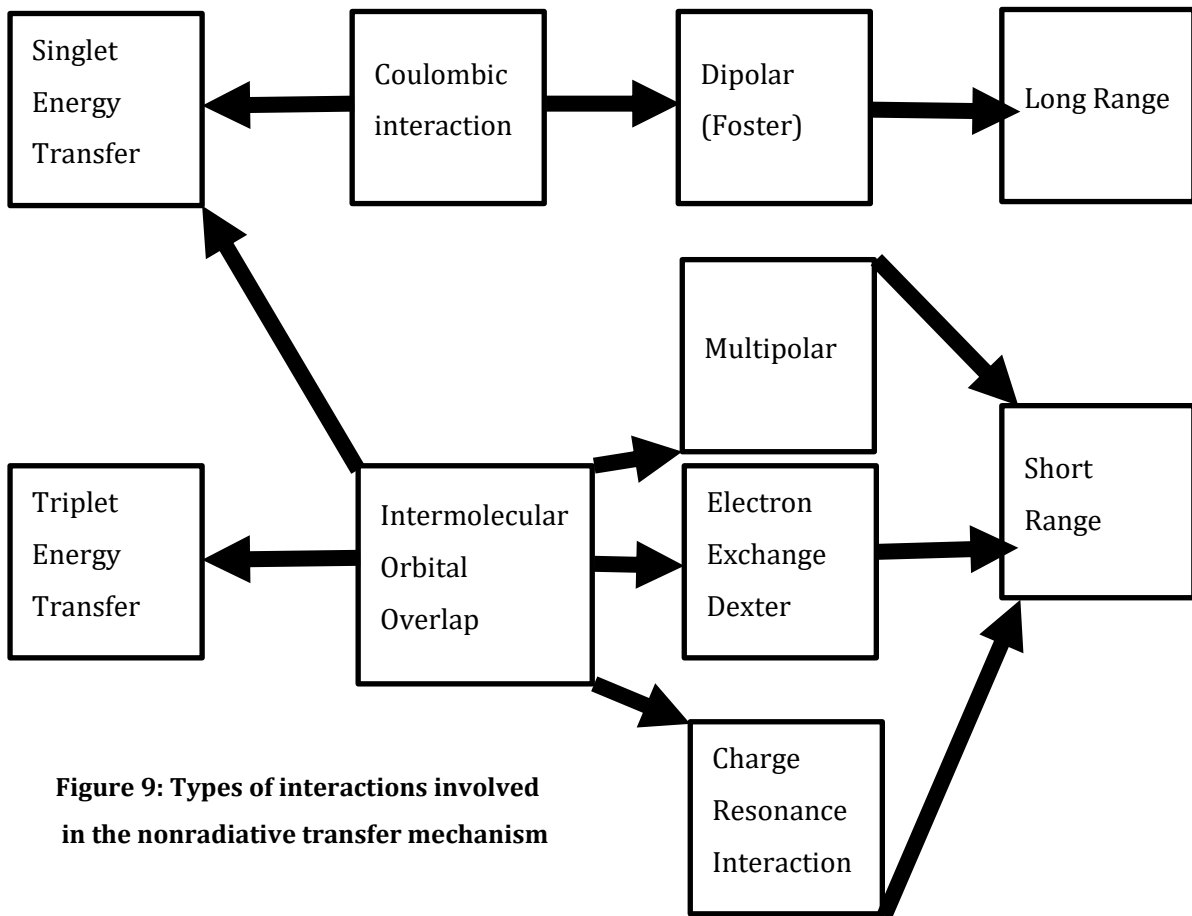


Figure 9: Types of interactions involved in the nonradiative transfer mechanism

2.6 Photoluminescence

Photoluminescence is light emission from any form of matter after absorption of photons (electromagnetic radiation). It is one of the many types of luminescence (light emission) and initiated by photoexcitation (i.e., photons that excite electrons to a higher energy level in an atom). After excitation, many different relaxation processes typically occur in which other photons radiate. The period between absorption and emission may vary ranging from short femtosecond-regime for discharge involving free carrier plasma in inorganic semiconductors up to milliseconds for phosphorescent processes in molecular systems, and under exceptional circumstances delay of release may even span to minutes or hours [12].

Photoluminescence spectroscopy is a contactless, non-destructive method of probing the electronic structure of materials. Light directed onto a sample, where it is absorbed and imparts excess energy into content in a process called photo-excitation. One way the specimen can dissipate this excess energy is through the emission of light, or luminescence [12].

2.6.1 NIR Fluorescence of SWCNTs for Optical Sensing

SWCNT are widely used in a variety of biomedical imaging modalities, including optical imaging, magnetic resonance imaging, and nuclear imaging. The magnetic and nuclear imaging rely mainly on the external labels or impurities in the CNT samples for imaging contrast. The focus here is the utilization of the inherent physical properties of the SWCNTs for optical imaging in biological systems [1].

The intrinsic optical properties of SWCNTs offer unique opportunities for optical biosensing. First, semi-conducting SWCNTs fluoresce at NIR wavelengths (900-1600). This wavelength range is within the “tissue transparency window,” in which the optical absorption of biological tissues is minimal, bounded by haemoglobin and water absorption. SWCNT-based optical biosensors operated at these NIR wavelengths could outperform conventional optical biosensors operated at visible wavelengths because blood cells and tissues are strongly absorbing and auto fluorescent at visible wavelengths. Second, the fluorescence of SWCNTs does not photobleach, and the intensity of the of the fluorescence does not fluctuate. Thus, SWCNT-based sensors could persist indefinitely, ideal for long-term sensing. In comparison, most conventional fluorophores emit fluorescence at visible wavelengths and rapidly photobleach or fades, limiting their applications [1].

2.7 Ultraviolet/Visible/Near Infrared (UV/VIS/NIR) Spectroscopy

UV/VIS/NIR spectroscopy is the most accepted systematic approach because of the versatility and ability to detect almost every molecule. This spectroscopy method uses UV/VIS/NIR electromagnetic radiation, the light is passed through a sample and the transmittance of light by the sample is measured. The absorbance can be calculated from the transmittance (T). An absorbance spectrum that is obtained shows the absorbance of a compound at different wavelengths. The amount of absorbance at any wavelength is due to the chemical structure of the molecule [13].

UV/VIS/NIR spectroscopy can be used in a qualitative manner, to identify functional groups or confirm the identity of a compound by matching the absorbance spectrum. It can also be used in a qualitative fashion, as the concentration of the analyte is related to the absorbance using Beer’s law, $A = \epsilon bC$ where ϵ is the molar attenuation coefficient, b is path length, and C is concentration. [13]

UV/VIS/NIR spectroscopy is used to quantify the amount of DNA or protein in a sample for water analysis, and as a detector for many types of chromatography. Kinetics of chemical

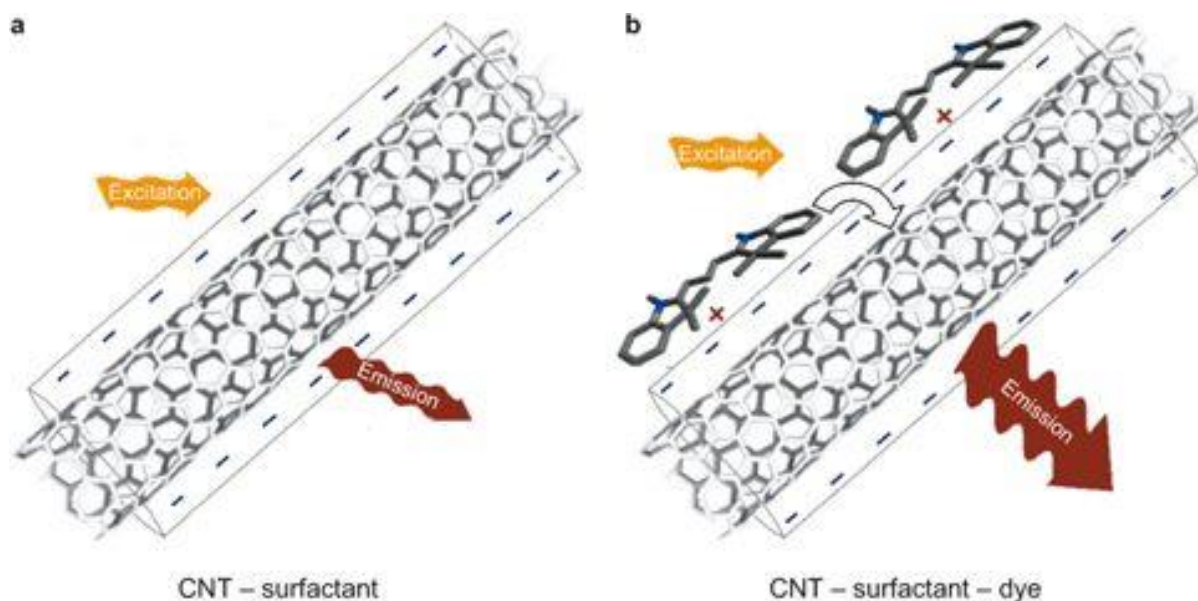


Figure 11 – (a) The addition of a surfactant to the CNT helps in forming a micelle around it. (b) The mixture of CNT-surfactant and dye results in Coulomb attraction between the positively charged dye molecule of astraphloxin and CNT micelle [2].

CNT-surfactant systems (Figure 11a) have very low photoluminescence. In the mixture of CNT with astraphloxin strong amplification of photoluminescence (up to 6 times) was observed from the nanotube levels in NIR range (Figure 11b). Thus, efficient energy transfer occurs from the astraphloxin to the tubes [2,16]. Other types of polymethine dyes were explored in study of energy transfer from the dye to CNT, and one of the most interesting results were obtained for the dioxaborine-cyanine dye (DOB-719) [17,18]. CNT with DOB-719 have efficient energy transfer photoluminescence with amplification more than an order of magnitude. Therefore, study of new modifications of cyanine dyes for functionalization of CNTs could improve the amplification of the nanotube emission further.

2.9 Dye - (Bis-astraphloxin)

Molecular structure of bis-astraphloxin is shown in Figure 12. This molecule consist of two astraphloxin units joined by a short linker (Figure 12). Our expectation is that the bis-astraphloxin could form a double layer – shell around the CNT resulting in enhanced photoluminescence (PL). This would improve the prospects of dye-CNT applications in imaging and the nanotube detection.

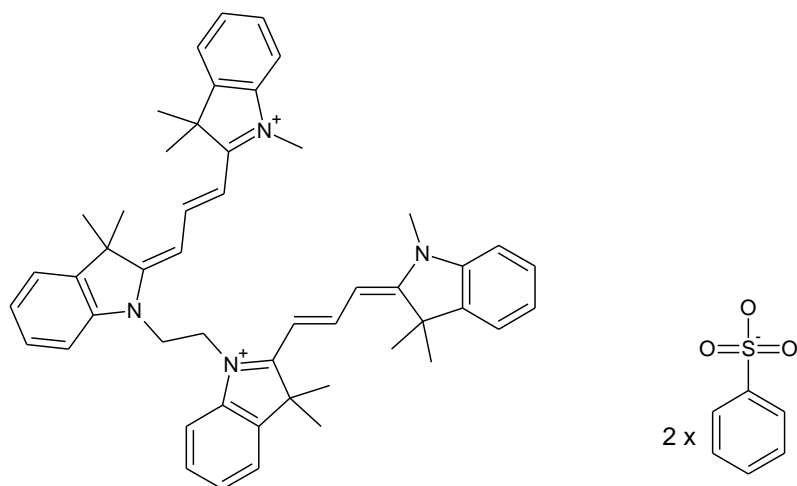


Figure 12 - Molecular structure of bis-astraphloxin formed as double molecule of astraphloxin, the negatively charged counter-ion on the right-hand side is added to stabilize positively charged bis-astraphloxin.

2.10 Surfactant - (SDBS)

One of the contributing factors that affect photoluminescence amplification is the type of ionic surfactant used. Therefore, SDBS as an essential surfactant is used in the experiment because of its high efficiency and prolonged stability in dispersing SWCNTs and thus yielding stable de bundled nanotubes in water [2].

Table 3: Different sample mixtures and volume measurements for the SWNT-surfactant-dye

CNT (20%)	Dye (0.0005 g/L)	H_2O	Total Volume
0.6 mL	0.015 mL	2.385 mL	3 mL

CNT (20%)	Dye (0.001 g/L)	H_2O	Total Volume
0.6 mL	0.03 mL	2.37 mL	3 mL

CNT (20%)	Dye (0.002 g/L)	H_2O	Total Volume
0.6 mL	0.06 mL	2.37 mL	3 mL

CNT (20%)	Dye (0.004 g/L)	H_2O	Total Volume
0.6 mL	0.12 mL	2.28 mL	3 mL

CNT (20%)	Dye (0.008 g/L)	H_2O	Total Volume
0.6 mL	0.24 mL	2.16 mL	3 mL

3.2 Absorption Characterization Experimental Setup

The Lambda 1050 UV/VIS/NIR (Perkin Elmer) spectrometer shown in Figure 13 was used during the experiment to measure the absorption spectra in the UV/VIS/NIR.



Figure 13 - Photo of the Perkin Elmer 1050 Spectrometer with the sample compartment in the closed position and detector module installed.

For scientific explanation, Figure 14 has revealed the schematic setup of the Perkin Elmer Lambda 1050 spectrophotometer. The Lambda 1050 UV/VIS/NIR spectrophotometer is a double slit spectrometer. Measurements made in a spectral range from 250 nm to 1400 nm, which is covered by two lamps. The location of the two lights is shown in Figure 14 above. A deuterium lamp D_2 for UV section and a tungsten lamp W for the visible and NIR spectral regions. For absorption spectra, measurements in the visible and NIR ranges the tungsten lamp was used. The tungsten lamp produces, like the incandescent light bulbs, a continuous spectrum from the near UV throughout the rest of the spectral range. The light was imaged through a slit assembly towards a set of filters and two consecutive monochromators which use holographic gratings. The monochromators filter a fraction with a small bandwidth. The light beam continues through a common beam mask (CBM), which can set the spot size. The CBM depolarizer follows, which can be included in the measurements if required. Thereafter, the light beam is separated into the reference beam and sample beam by a chopper, consisting of a rotating disc with a mirror and a window segment directing the beam in either direction. The two beams are then directed through the sample compartment of the spectrometer, where the samples are placed in either path. The detector module installed at the end of the schematic diagram for detection [13].

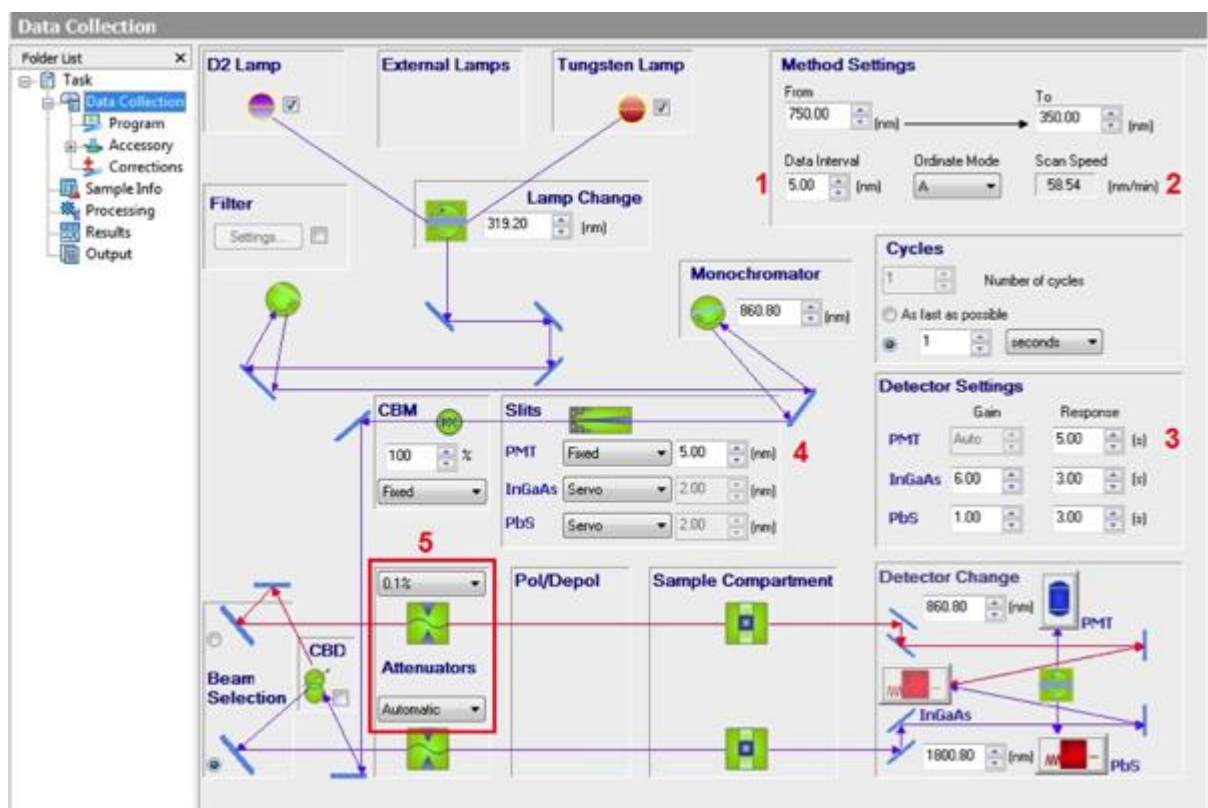


Figure 14 – Path of light through the schematic setup of the Perkin Elmer Spectrometer.

3.3 Photoluminescence (PL) Characterization

Experimental Setup

The fluorescence emission spectra at various excitation wavelengths were recorded using Horiba NanoLog excitation – emission spectrofluorometer equipped with nitrogen – cooled InGaAs array detector to generate PL excitation-emission maps as in Figure 15.



Figure 15 – Fluorescence Spectrometer

Figure 16 represents a simplified diagram of a spectrofluorometer for the purpose of comprehension.

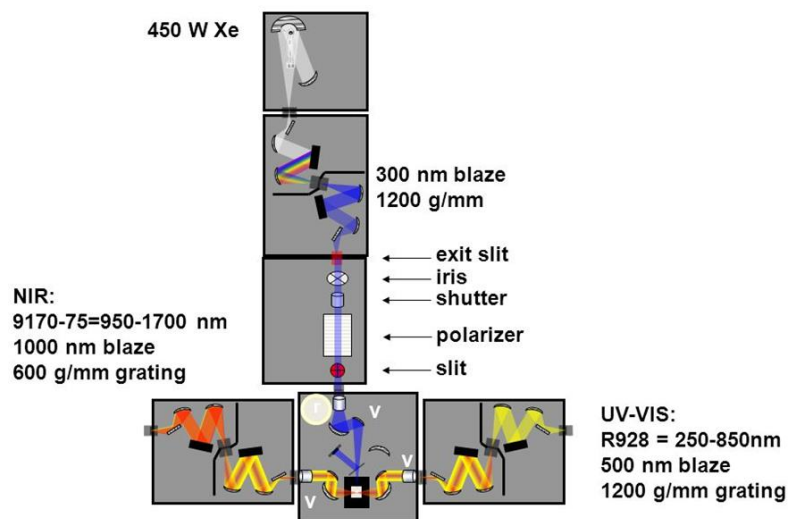


Figure 16 – Fluorolog – 3 Spectrofluorometer

Such system allows to record PLE maps, where excitation wavelength (λ_{EX} or EX wavelength) is plotted on the Y-axis, emission wavelength (λ_{EM} or EM wavelength) on the X-axis, and PL intensity represented as a contour map. The highest intensity is shown in red, whereas blue colour shows the lowest PL intensity.

The 450 W excitation is the source of radiation for producing photons. The beam of light that comes from the lamp is filtered by an excitation monochromator that allows only a single wavelength of light to reach the sample. The sample compartment module is a T- box, which provides efficient throughput with a choice of standard right - angle emission collection. The sample compartment module comes equipped with a silicon photodiode reference detector to monitor and compensate for variations in the source output. The emission from the sample is filtered by an emission monochromator that feeds the signal to a photomultiplier detector. By stepping either or both monochromators through a wavelength region and recording the variation in intensity as a function of wavelength, a spectrum gets produced [8]. The monochromator, sample - compartment unit and accessories are all connected to a controller called the SpectrAcq, which transfers information to and from the host computer.

4 Experiments

For absorption and photoluminescence characterization, the experiments were conducted by first measuring absorption spectra in the visible and NIR ranges for the samples and second by measuring the fluorescence emission spectra in the NIR or visible ranges for the initial CNT, diluted CNT (20% CNT and 80% water), mixtures of SWCNTs and dyes (bis-astraphloxin or astraphloxin) at various concentrations (Table 3).

4.1 Measuring Absorption

After sample preparation as can be seen in Figure 17. The absorption spectra in the visible and NIR ranges are measured by using the Lambda 1050 UV/VIS/NIR spectrometer and a host computer.

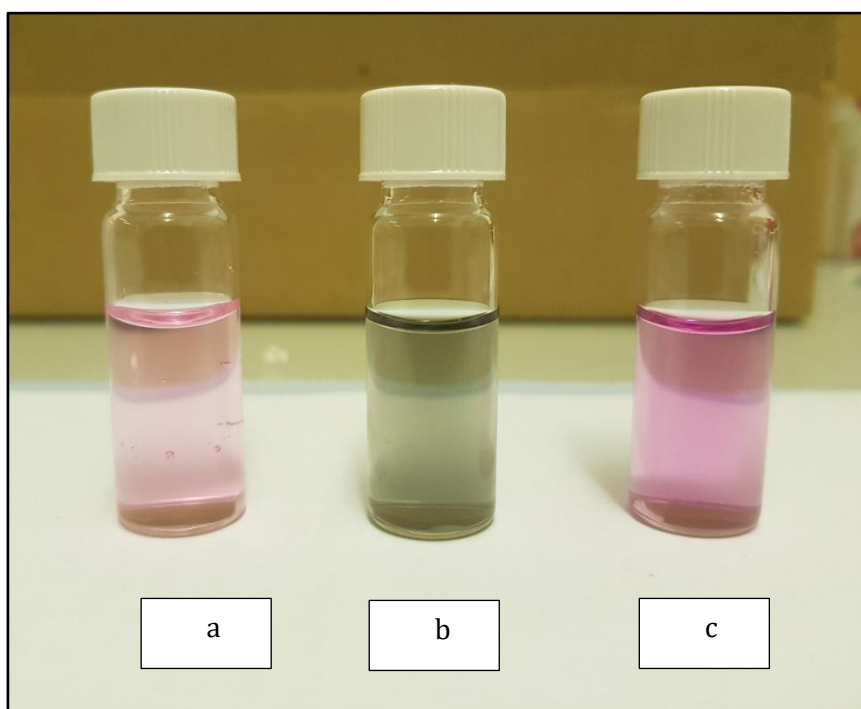


Figure 17 - Prepared samples (a) Mixture of CNT + Bis-Astra 0.001 g/L, (b) CNT - surfactant (c) Mixture of CNT + Bis-Astra 0.004 g/L

The process of setting the parameters for measuring the absorptions spectra comes after all the devices and accessories are connected to the host computer as shown in Figure 14. The procedures involved are listed below.

1. Calibration of the spectrometer to establish zero line (or 100% transmission)

2. Performing immediate measurements of an absorption spectrum
3. Performing delayed measurements of an absorption spectrum

4.1.1 Zero-line calibration of the spectrometer

Calibration of zero-line is an essential element for accurate measurements to be achieved. The step-by-step procedure taken to calibrate the spectrometer without samples was straight forward and described below.

- Turned on the spectrometer and allowed the lamp to warm up for an appropriate time (about 15 to 20 minutes) for stabilization of the system.
- Double clicked PerkinElmer on the desktop of the host computer
- Clicked on Scan lambda to begin data collection and method settings set between 1400 nm (infrared) to 250 nm (UV).
- The data interval set to either 1 or 1.50 (steps) depending on the sample
- Clicked on sample information to set the number of samples
- Clicked start for zero line

4.1.2 Immediate Measurements of Absorption

Before measuring, each sample was freshly prepared and placed in a sample cell for instant measurements. The absorption spectra of each sample were collected by setting the parameters and placing the sample cell in the sample compartment and deionized water as a reference sample which was placed in the reference sample compartment. Both samples are cleaned of any fingerprints. The sample cell and the sample compartment are properly closed to prevent any ambient light. Collected an absorption spectrum by allowing the device to scan through different wavelengths and collected the absorbance. From the collected spectrum, the absorbance maxima were determined (λ_{\max}). Repeated the collection of spectra to get estimated error in the (λ_{\max}).

4.1.3 Delayed or Temporal Measurements of Absorption

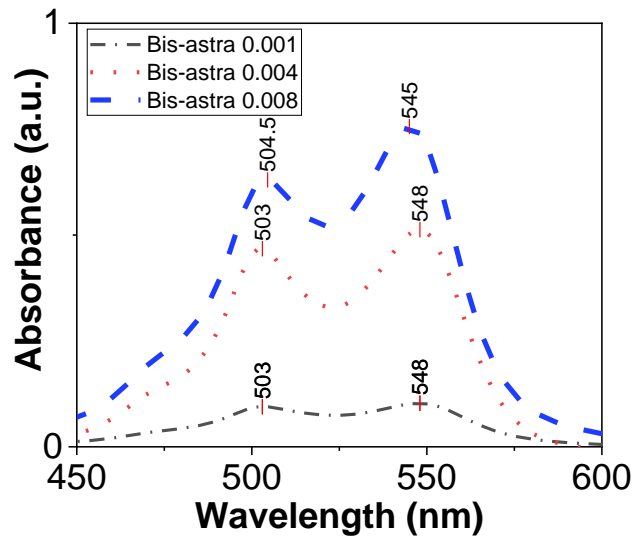
The same technique of measuring samples in “immediate measurements” are applied to delayed measurements as well, except that the sample cells are aged over time and measured to investigate the behaviour of the systems and the energy transfer that takes place after few days to a week.

4.2 Results

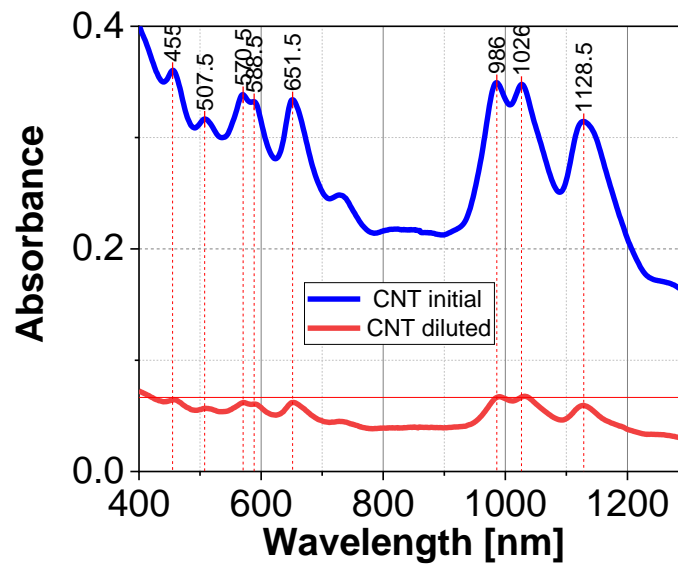
4.2.1 Immediate Measurement of Dye and CNT

The absorption spectra of the dyes and CNTs as seen in Figure 18, were first taken to gain some essential information about each concentration.

a)



b)



c)

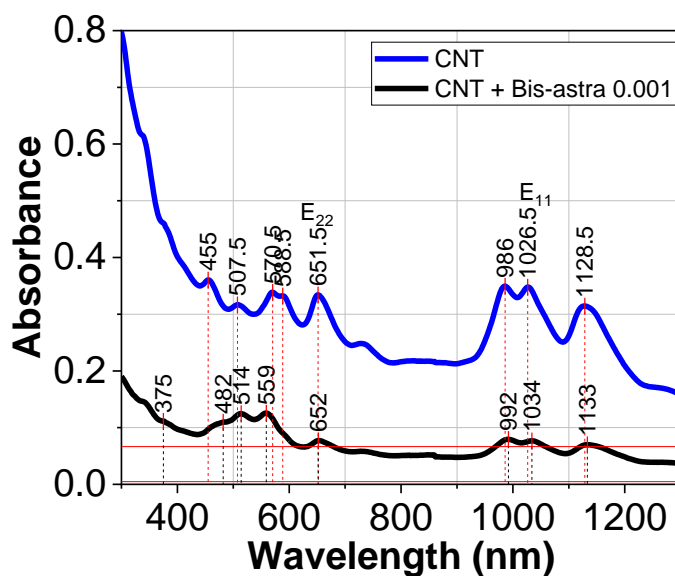
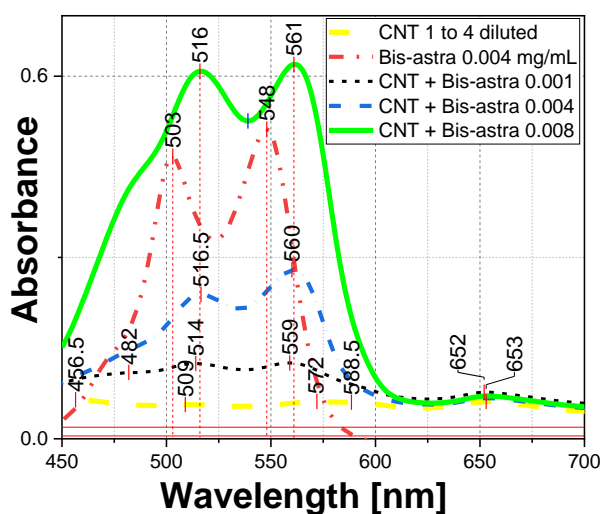


Figure 18 - (a) Absorption spectra of water solutions of bis-astraphloxin (0.001 mg/mL, 0.004 mg/mL, 0.008 mg/mL). (b) Absorption spectra in the visible and NIR ranges of neat CNT dispersions: stock dispersion in blue and diluted 1:4 in red. (c) Mixture of CNT with bis-astraphloxin (0.001 mg/mL) in black and stock dispersion of CNT in blue. The CNTs dispersed in water with SDBS.

4.2.2 Immediate Measurement of the Mixtures

The two absorption graphs in Figure 19, illustrated results for the freshly prepared diluted CNT, bis-astraphloxin, astraphoxin, mixtures of bis-astraphloxin + CNT and mixtures of astraphloxin + CNT.

a)



b)

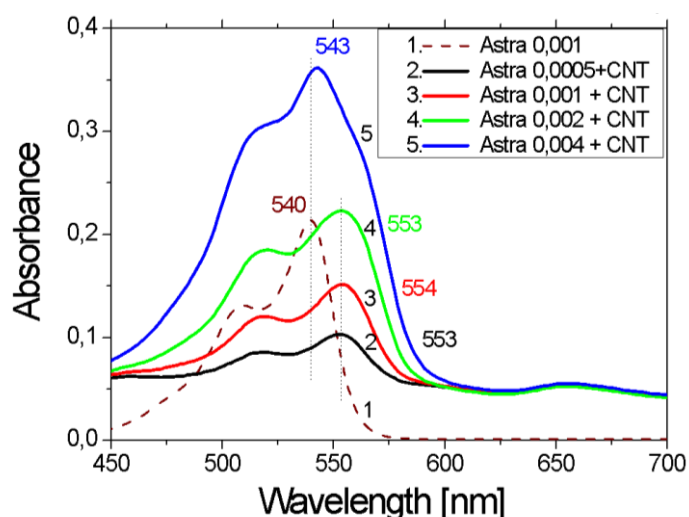


Figure 19 - Absorption spectra of bis-astrophloxin, astrophloxin and SWCNTs dispersed with SDBS. (a) Absorption spectra of a mixture of 20 % CNT and 80% water (CNT 1 to 4 diluted) as reference, spectra of water solution of bis-astrophloxin (0.004 mg/mL), mixtures of CNTs with bis-astrophloxin (0.001 mg/mL, 0.004 mg/mL, 0.008 mg/mL, where the concentrations given here are the dye concentrations in the mixture). (b) Absorption spectra of water solution of astrophloxin 0.004 mg/mL, mixtures of CNTs with astrophloxin (0.0005 mg/mL, 0.001 mg/mL, 0.002 mg/mL, 0.004 mg/mL, here again the concentrations given are the dye concentrations in the mixture).

4.2.3 Delayed/Temporal Measurement Results

Since the focus in this experimental research is to investigate energy transfer in the new system of CNT-surfactant-dye(bis-astrophloxin), that is expected to show an exceptional magnification of photoluminescence response via energy transfer and such attributes have many practical or industrial applications. The need to investigate energy transfer overtime is also very paramount and Figure 20 illustrates the absorption spectra of the samples after a few days to a week or more.

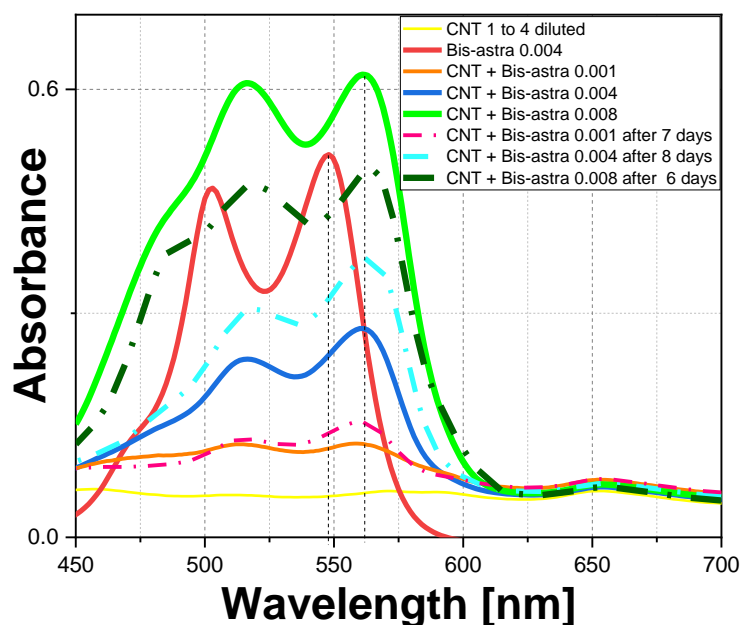


Figure 20 -Absorption spectra of a mixture of 20 % CNT and 80% water (CNT 1 to 4 diluted) as reference, spectra of water solution of bis-astraphloxin (0.004 mg/mL), mixtures of CNTs with bis-astraphloxin (0.001 mg/mL, 0.004 mg/mL, 0.008 mg/mL, where the concentrations given here are the dye concentrations in the mixture). the mixtures of CNTs with bis-astraphloxin (0.001 mg/mL, 0.004 mg/mL, 0.008 mg/mL, where the concentrations are the dye concentrations in the mixture) aged over days to a week to investigate the energy transfer.

4.3 Discussion/Analysis

The absorption spectra of bis-astraphloxin solutions as shown in Figure 18 (a), exhibit a maximum at $\lambda_M = 548$ nm and a vibrational progression band at 503 nm for the two lower concentrations (0.001 mg/mL, 0.004 mg/mL). The absorption spectrum of bis-astraphloxin at higher concentration (0.008 mg/mL) has a blue-shifted $\lambda_M = 545$ nm evidencing tendency for H-type aggregation of bis-astraphloxin molecules at high concentration. It should be noted that H-aggregate molecular alignment was observed for astraphloxin at much higher concentration [16]. This type of aggregation is ideally non fluorescent in nature. Normally such aggregation behaviour of fluorescent dye molecules strongly quenches their fluorescence, which has an adverse effect in designing display devices and sensors as this application are mainly based on the fluorescence properties. Therefore, it is very crucial for the applicability of these fluorescent dyes either to control aggregation or to get fluorescent signal from these aggregates. Aggregation of the dye molecules can be controlled by mixing these dyes with different materials [1, 16].

Figure 18 (b,c) illustrates experimental evidences for the interaction of bis-astraphloxin with CNT due to comparison of absorption spectra of neat CNT and mixture of CNT with the dye. The interaction is evidenced by the absorbance data in the field of transparency of the dye (600-1250nm): by analysing the excitonic peaks E_{11} (900 nm – 1250 nm) and E_{22} (550 nm -750 nm) in the CNT absorption spectra and the mixtures. It was observed that the high-energy E_{22} peaks of the CNTs with its maximum at 652 nm, remains fixed in position. Whereas, the low energy E_{11} bands peaked at 986 nm, 1026.5 nm and 1128.5 nm for neat CNT are red-shifted to 992 nm, 1034 nm and 1133 nm in the mixtures, respectively.

Experimental results for the immediate measurements displayed in Figure 19 (a) for CNT, bis-astraphloxin, and mixtures of CNT with bis-astraphloxin indicates the complexation of bis-astraphloxin with CNTs. The absorption spectra for the combinations of bis-astraphloxin with CNTs contained strongly red-shifted dye absorption peaks. The extent of the red-shift depends on the dye concentration. The strongest red shift was observed for dye concentration 0.008 mg/mL peaking at $\lambda_M = 561$ nm. The red-shifted absorption bands in the range of 555-600 nm referenced to J-like aggregates of bis-astraphloxin. We observe no peak of the monomers ($\lambda_M = 548$ nm) in the spectra of the mixtures. Thus, all molecules of bis-astraphloxin in the studied mixtures are interacting with CNT, and no monomers are present in the mixtures. We have compared the results for the mixtures with bis-astraphloxin and mixtures with astraphloxin. The mixture of CNT with astraphloxin molecule also illustrated the complexation of astraphloxin with CNTs as was observed previously [2,16]: the absorption spectra for the mixtures indicates red-shifted dye absorption peaks. However, the extent of the red-shift depended on the dye concentration. Importantly, the monomer molecules of astraphloxin at $\lambda_M = 540$ nm appear in the mixtures at concentration of 0.004 mg/mL. By observing the threshold in the appearance of the dye monomer, which falls in the range of 0.002-0.004 mg/mL, suggests that the astraphloxin covers the surface of the CNTs in a single layer. Considering that all bis-astraphloxin molecules interact with the nanotubes at much higher concentration, we assume that bis-astraphloxin is covering CNT with multi-layered shell: two or even more layers. This could be attributed to complex molecular structure of bis-astraphloxin molecules.

Temporal or delayed measurements of the absorption spectra of the neat dye (bis-astraphloxin or astraphloxin) and neat CNT dispersions aged over a week did not show any changes in the spectra (Figure 20). Besides, the mixtures of CNT-bis-astraphloxin did indicate some significant changes over time. The absorption of mixtures with low concentration (0.001 mg/mL) of the dye grows and is slightly red-shifted, when aged over a week. A mixture of CNT-bis-astraphloxin at 0.004 mg/mL aged over eight days manifested a considerable increase in the absorption intensity and the peaks are slightly red-shifted. Finally, the mixture at high concentration of the dye (0.008 mg/mL) when aged over six days behaves differently and

instead decreases in absorption intensity. Such changes could be explained by improved complexation with time for the dye molecules at the concentrations equal and below 0.004 mg/mL. Oppositely, at higher concentrations (above 0.004 mg/mL) the process of dye complexation on the nanotubes could be interfered by creation of heavily covered CNT-dye systems, which start to form bundles. Such dynamics could be confirmed by PL measurements for aged samples of the mixtures.

4.4 Measuring Fluorescence Emission/ MAPS

As soon as samples were prepared as shown in Figure 17, the next procedure on measurements using the fluorescence spectrometer (Figures 15,16) was followed:

1. Fluorescence system calibration
2. Immediate measuring of samples in the VIS/NIR
3. Delayed/Temporal measurements of Samples in the VIS/NIR

4.4.1 Fluorescence Spectrometer System Calibration

The fluorescence spectrometer has two calibration checks that need to be done before running any measurements. This check helps to prevent errors in the measurements. The device is calibrated by conducting an excitation and emission calibration check. The excitation calibration check verifies the wavelength calibration of the excitation monochromator, using the reference photodiode located before the sample compartment. It is an excitation scan of the Xenon lamp output and should be a very initial check. The second calibration check is the emission check of the instrument, and it is directly affected by the calibration of the excitation monochromator. The emission calibration verifies the wavelength calibration of the emission monochromator with the emission photomultiplier tube.

4.4.2 Immediate measurement of Samples in VIS/NIR

The method of measuring in the visible and near infrared comes after all other system checks are conducted and indicating that the system is running correctly and no significant issues. The procedures adopted for measurements in both the visible and infrared are described below.

- Inserted a sample cell in the sample compartment and closed the lid of the compartment properly to avoid ambient light interfering with the specimen.
- Doubled clicked on the Icon on the desktop
- On the main FluorEssence toolbar, Selected the experiment menu button “**M**”. This opens the main experiment window
- Selected the spectra button for the experiment type window to appear

- Specified by choosing either excitation or emission depending on what the measurement was. Then clicked the next button.
- Adjusted the default parameters for the monochromator depending on the measurement.
- Clicked the Run button “**Run**”

Table 4 and Table 5 below indicate the setting parameters for performed measurements in either the NIR or visible range.

Table 4: Settings for PL measurements in the visible range

Monochromator parameters for measurements in the visible range				
Monochromator (1200 grooves/mm)	Initial Wavelength	Final wavelength	Increment	Slits
Excitation	400 nm	700 nm	5 nm	2 nm
Emission	450 nm	800 nm	5 nm	2 nm

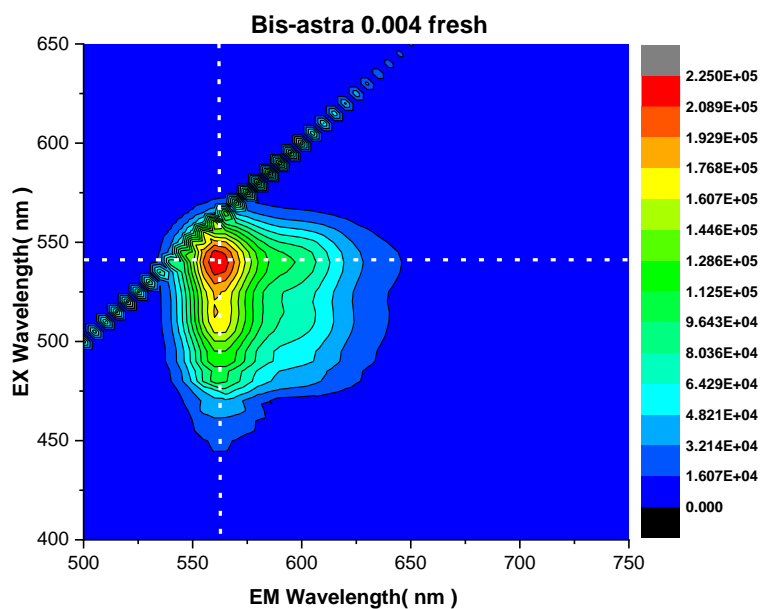
Table 5: Settings for PL measurements in the infrared range

Monochromator parameters for measurements in the infrared range				
Monochromator (1200 grooves/mm)	Initial Wavelength	Final wavelength	Increment	Slits
Excitation	300 nm	800 nm	5 nm	10 nm
Emission	900 nm	1400 nm	5 nm	10 nm

4.5 Results

4.5.1 Immediate Measurement of PLE Maps of Bis-astraphloxin and Astraphloxin

a)



b)

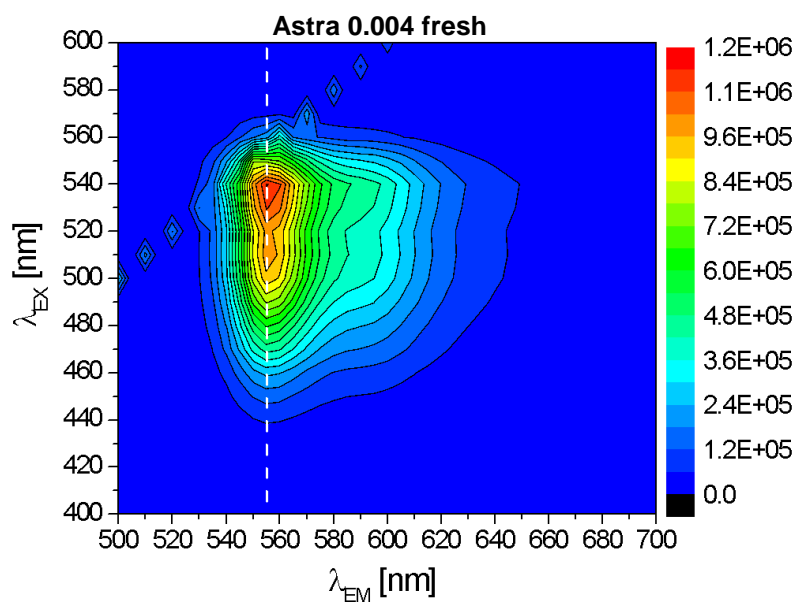
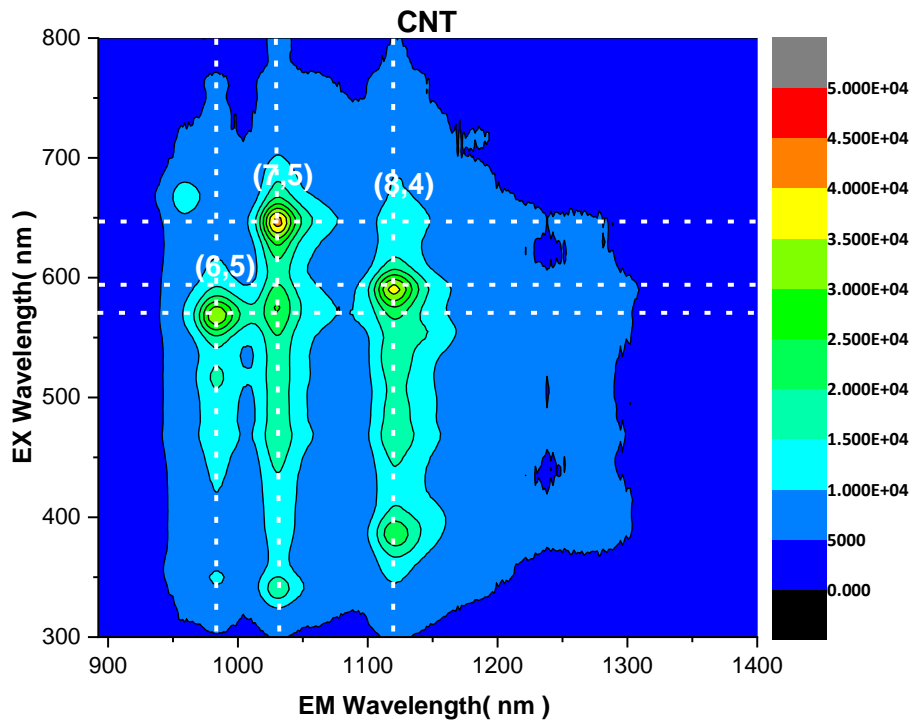


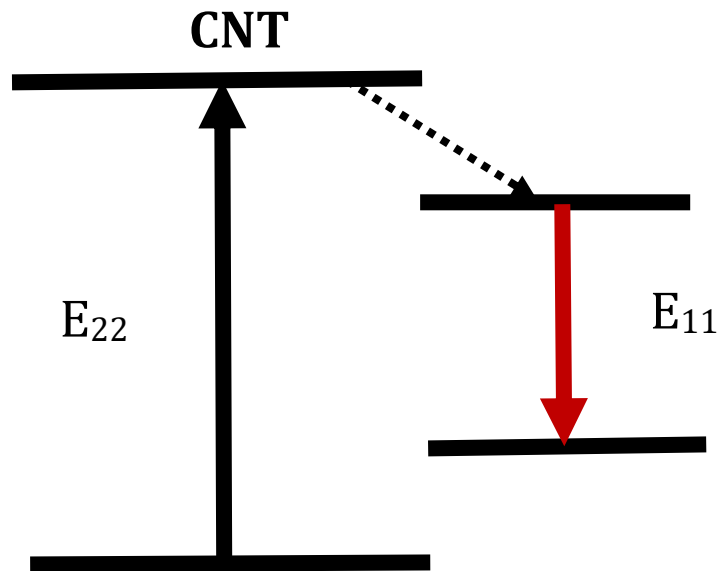
Figure 21 - PLE maps for the dyes in visible range at concentration 0.004 mg/mL: (a) bis-astraphloxin and (b) bis-astraphloxin.

4.5.2 Neat CNT and A Mixture of CNT with Bis-astrophloxin

a)



b)



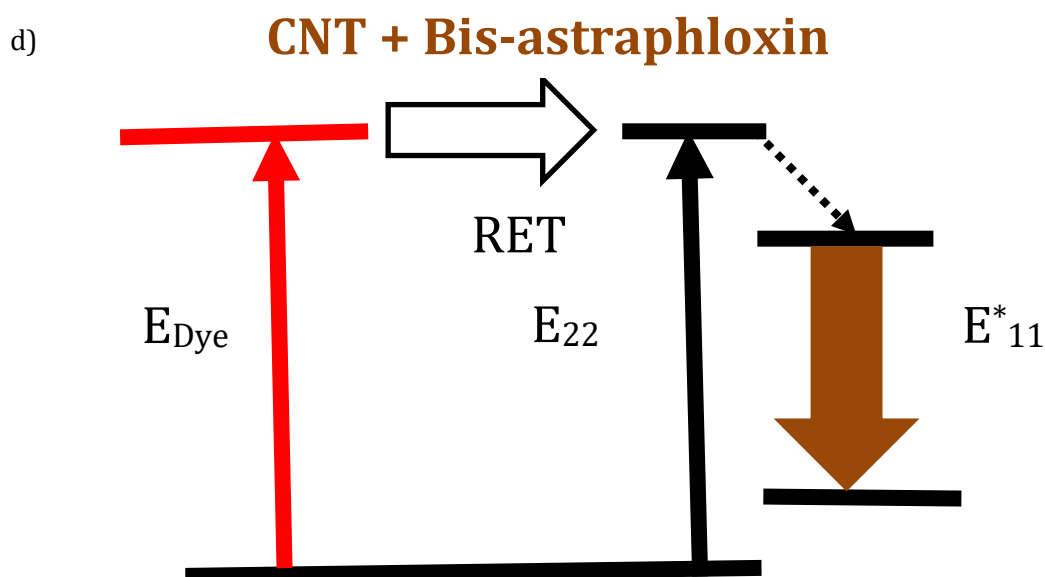
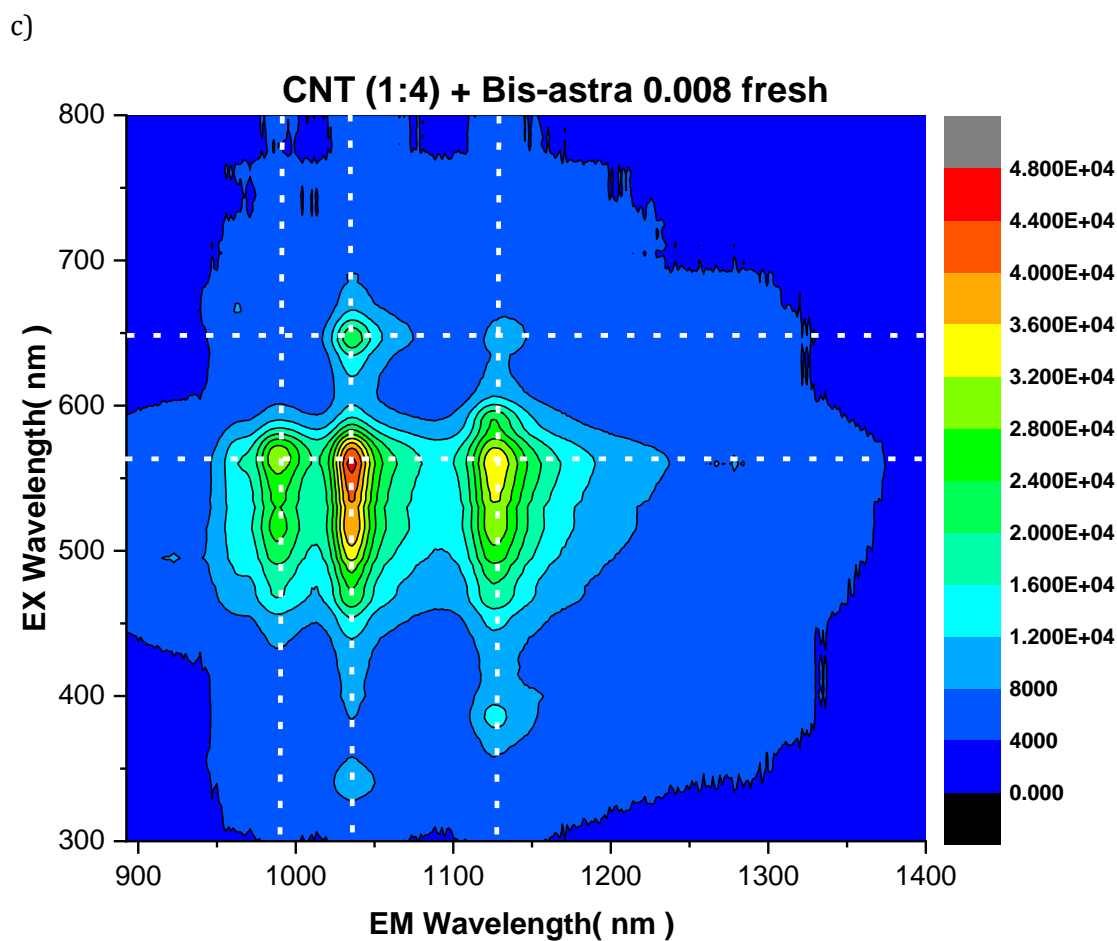
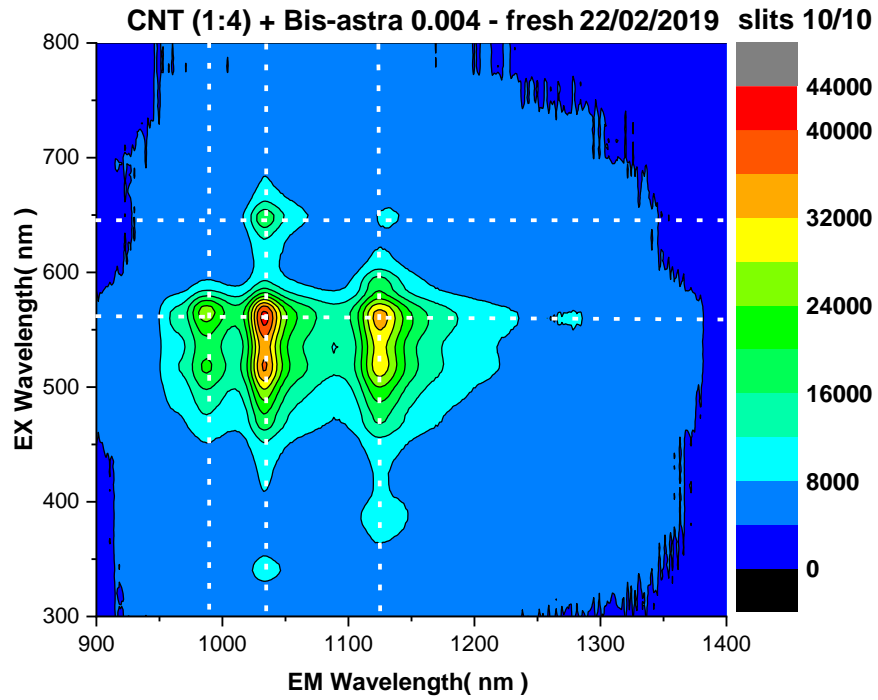


Figure 22 - PLE map for water solutions of (a) neat CNTs dispersed with SDBS. (b) Energy diagram indicates that (a) CNTs have specific exciton energy levels of PL excitation (E_{22}) and emission (E_{11}) in the visible and NIR ranges, respectively. (c) PLE map for a mixture of CNTs with bis-astraphloxin (0.004 mg/mL) (d) a visible-range excitation of the dye molecules (E_{Dye}) attached to the nanotubes is transferred via RET to these CNT levels (E_{22} with subsequent relaxation to E^*_{11} in the NIR range).

4.5.3 Mixtures of CNT with Dyes.

a)



b)

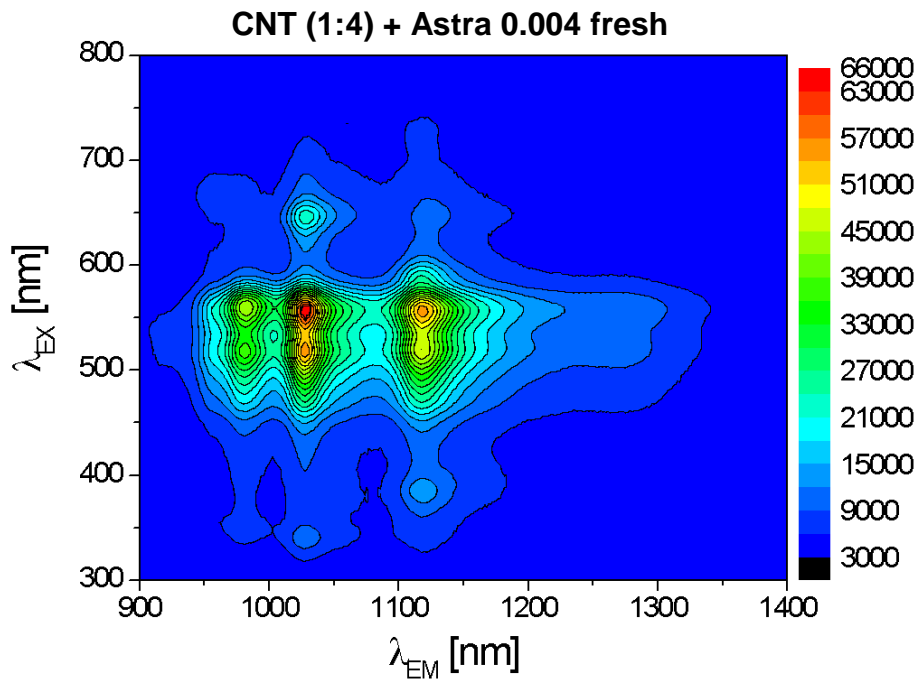
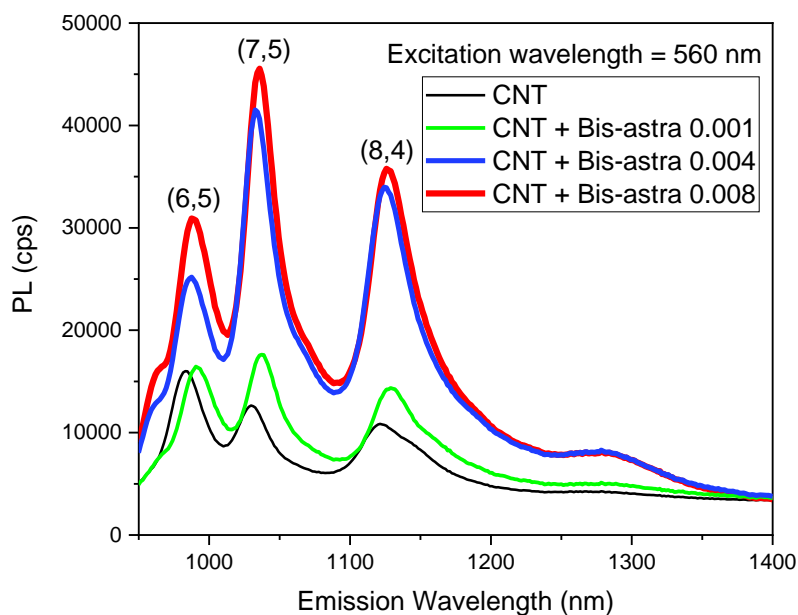


Figure 23 – PLE maps for the mixtures of CNTs with dyes at concentration of 0.004 mg/mL: (a) bis-astraphloxin and (b) astraphloxin.

4.5.4 PL Spectra of Neat CNT and the Mixtures

a)



b)

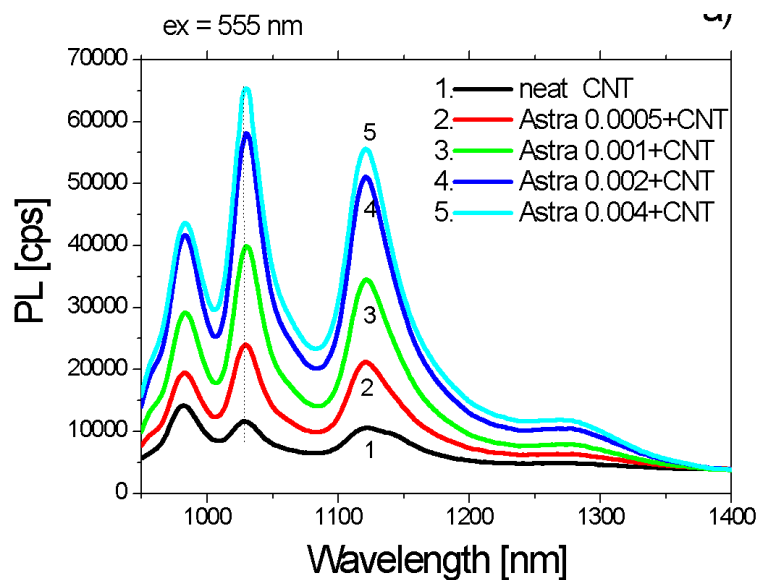
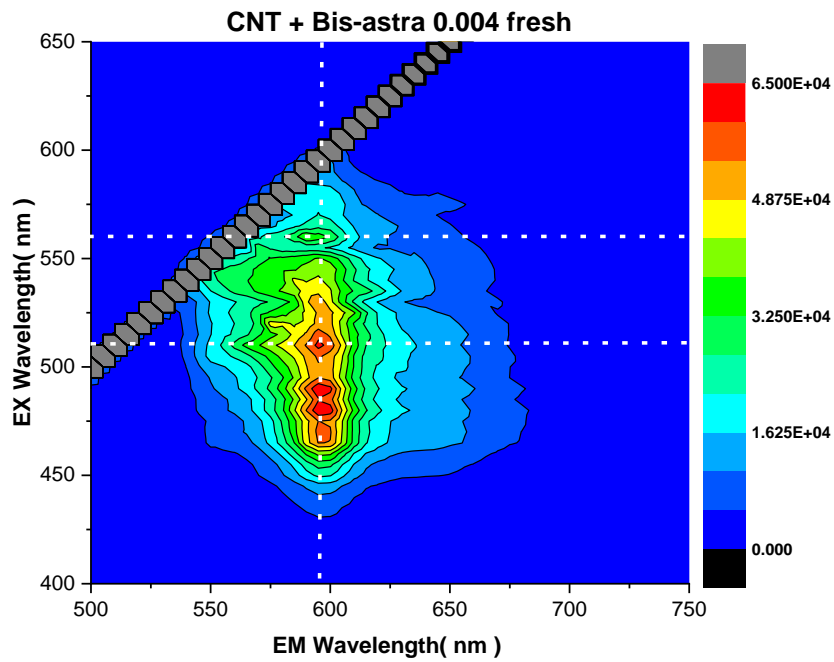


Figure 24 - Dependence of PL on organic dye concentration in the mixtures with CNTs. (a) PL spectra of water solutions of neat CNTs and mixtures of CNTs with bis-astraphloxin (0.001 mg/mL, 0.004 mg/mL, 0.008 mg/mL). (b) PL spectra of water solutions of neat CNTs and mixtures of CNTs with astraphloxin (0.0005 mg/mL, 0.001 mg/mL, 0.002 mg/mL, 0.004 mg/mL).

4.5.1 A Mixture of CNT with Bis-astrophloxin Measured Fresh and Measured After a Week

a)



b)

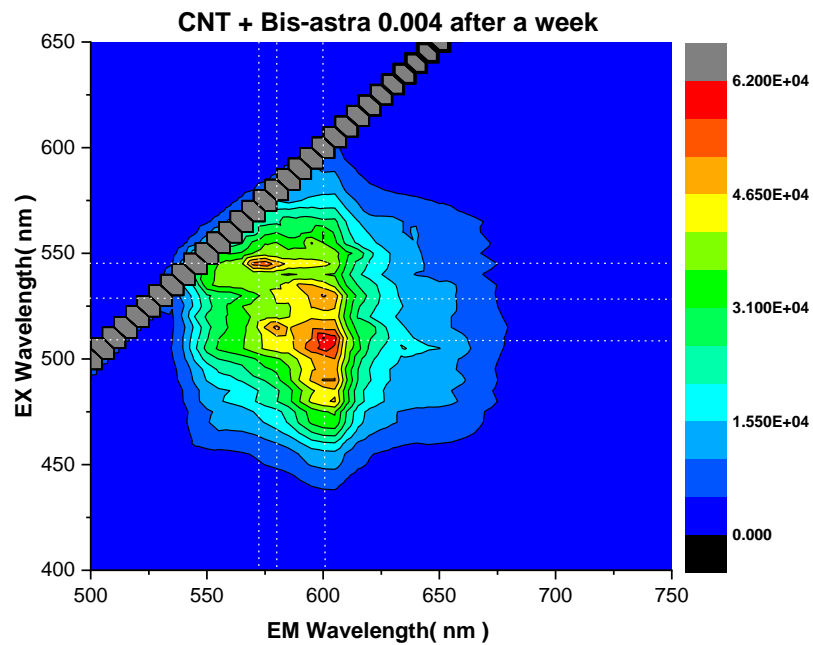


Figure 25 – PLE maps for the mixture of CNT with bis-astrophloxin (0.004 mg/mL): (a) fresh and (b) after a week.

4.6 Discussions/Analysis

In the visible range, the measured PL excitation-emission (PLE) maps for the neat bis-astraphloxin and astraphloxin (both 0.004 mg/mL) as in Figure 21 indicates a maximum intensity of 2.3×10^5 and 1.2×10^6 , respectively. It should be noted, that the astraphloxin has much higher PL intensity than the bis-astraphloxin of the same concentration. For both dyes is practically the same: $\lambda_{EX} = 540$ nm, however $\lambda_{EM} = 556$ nm for astraphloxin and $\lambda_{EM} = 565$ nm for bis-astraphloxin (Figure 21). Both accurate solutions of the dyes remained stable for weeks with no changes in intensity and aggregation formation.

The PL excitation-emission (PLE) maps measured in the NIR range for the neat CNTs and mixture of CNTs with bis-astraphloxin (0.008 mg/mL) are shown in Figure 22. The PLE maps for the neat CNTs (Figure 22a) with λ_{EX} at E_{22} , E_{33} , and E_{44} and λ_{EM} at E_{11} revealed the presence of CNTs with chiralities of (6,5), (7,5), (8,4) in the studied dispersions. The PLE maps of the mixtures of CNTs with bis-astraphloxin indicated a significant increase in the PL intensity from tubes of all chiralities (E_{11}^*) in the dye excitation range, with a maximum at $\lambda_{EX} = 560$ nm. The peak of λ_{EX} does not coincide with λ_M of bis-astraphloxin, the absorption maximum of the monomers (see Figure 19a). However, it does coincide with the absorption maximum for the interaction of the dye with the CNTs at all the three concentrations levels (0.001 mg/mL, 0.004 mg/mL and 0.008 mg/mL; see Figure 19a).

Similarly, the PLE maps of the mixtures of CNTs with astraphloxin also indicated a significant improvement in the PL intensity from all tubes of all chiralities (E_{11}^*) in the dye excitation range, with a maximum at $\lambda_{EX} = 555$ nm (Figure 23b). The peak of λ_{EX} does not coincide with λ_M as well (see Figure 19b), the absorption maximum of the monomers and mixtures at higher concentrations (0.002 and 0.004 mg/mL). Notwithstanding, it does coincide with the absorption maximum (554 nm) for the interaction of the dye with the CNTs at lower concentration (0.0005 mg/mL).

Therefore, resonant energy transfer (RET) from an excited molecule of dye (donor) attached to CNT (acceptor), a different molecule meaning hetrotransfer, is the most apparent cause of this effect and can be explained in terms of dipole-dipole interactions between the donor and acceptor. Moreover, the astraphloxin monomers present in the mixture at high concentration do not transfer energy to the CNTs, as seen from the absence of PL peaks at $\lambda_{EX} = \lambda_M = 540$ nm (Figure 23b). Whereas, the astraphloxin molecule at lower concentration (0.0005 mg/mL) and bis-astraphloxin molecule at all the three different dye concentrations (0.001 mg/mL, 0.004 mg/mL and 0.008 mg/mL) do transfer energy to the CNT as seen from the presence of PL peaks at $\lambda_{EX} = \lambda_M = 555$ nm and $\lambda_{EX} = \lambda_M = 560$ nm, respectively. This means that short-range energy transfer of the Direct charge exchange (Dexter type transfer) is more likely because it occurs at a closer proximity (<1 nm) than a Förster mechanism for RET, which is sensitive at distances of 1-10 nm between donor and acceptor molecules.

For the purpose of illustrating the intensification of CNT emission due to the energy transfer, the extracted PL emission spectra at $\lambda_{EX} = 560$ nm for the bis-astraphloxin and $\lambda_{EX} = 555$ nm for the astraphloxin from the PLE maps are shown in Figure 24(a) and Figure 24(b) respectively. The maximum PL enlargement of about 6 times was achieved at astraphloxin concentration of 0.004 mg/mL. Whereas, the maximum PL amplification was achieved at a bis-astraphloxin concentration of 0.008 mg/mL. Additionally, the PL spectra indicate the different effects of the dye on CNTs of each chirality, revealing selectively in the complexation with CNTs of various diameters (Figure 24).

According to Figure 24a, the PL intensity by the emission wavelength corresponding to a mixture of CNT with bis-astraphloxin of concentration 0.008 mg/mL and to neat CNTs of various chiralities – (6,5), (7,5), and (8,4), the highest (up to a factor of 4) PL amplification achieved for the (7,5) chirality. In addition, the PL intensity by the emission wavelength corresponding to a mixture of CNT with astraphloxin of concentration of 0.004 mg/mL and to neat CNTs of various chiralities – (6,5), (7,5) and (8,4), the highest (up to a factor of 6) PL amplification achieved for the (7,5) chirality (Figure 24b). The reason why the astraphloxin achieved a higher amplification than the bis-astraphloxin is believed to be due to more complex electronic structure of the bis-astraphloxin molecules.

Among the different CNT chiralities revealed in Figure 22a, the largest diameter or surface area corresponds to (8,4) chairality, which implies that a greater number of the dye molecules can complex with the CNTs for exhibiting the highest PL intensification, but it fails to achieve the peak PL amplification. This observation demonstrates that the electronic structure frameworks of both the CNTs and the organic dyes must simultaneously influence the PL magnification.

Comparison of the PLE maps in visible range for neat bis-astraphloxin (Figure 21a) and mixtures of the dye with CNT (Figure 25) shows aggregates formation with prominent red-shifted bands at $\lambda_{EM} = 600$ nm. In addition, the monomer emission becomes strongly quenched in such systems. The bis-astraphloxin aggregation in CNTs is featured by one peak ($\lambda_{EM} = 600$ nm), whereas the astraphloxin aggregation resulted in multiple peaks [16]. It evidences formation of one type of aggregates by bis-astraphloxin, and various types for astraphloxin system.

Temporal or delayed measurements of the PLE maps of the neat dye (bis-astraphloxin or astraphloxin) and neat CNT dispersions aged over a week did not show any changes in the spectra (Appendix). The mixtures of CNT-bis-astraphloxin have some significant changes over time in spectral shape. The NIR PL of mixtures with low concentration (0.001 and 0.004mg/mL) of the dye grows, when aged over a week. Oppositely, the mixture at high concentration of the dye (0.008 mg/mL) when aged over six days has lower PL intensity in NIR. Such dynamics correlate with the changes observed for absorption evidencing slightly improved complexation with time for the dye molecules at low dye the concentrations.

4.7 General Challenges and Mitigation

Since nanoscience field of research was a new thing to me and I was very inexperienced in this area of scientific research. It was at first a very challenging and I did not know where to start from. Therefore, after few meetings with my primary supervisor I started with a literature survey by devoting a lot of time into reviewing articles and focusing mainly on the key subjects related to this project.

Familiarizing myself with the laboratory equipment and understanding the working principles of the absorption and photoluminescence spectrometers through training was not just straightforward. Carrying out sample preparations and running measurements was very demanding. I had to put in lots of time to comprehend the experimental techniques of running sample measurements. Data analysis using OriginLab software was not an easy task, as it was a completely new platform. I spent lots of time by reading and watching videos to understand how the programme works. OriginLab turned out to be an excellent platform of choice for data analysis and graphing. It enabled an easy-to-use interface for beginners without the need for a written language. The software provided an essential set of tools for performing exploratory and advanced analysis of data.

Due to the number of people that uses the spectrometer for other research experiments, I find it very hard at times to take immediate or delayed measurements and this did not help me to achieve the time and date a certain measurement needs to be taken. Therefore, I must wait for the next day in some instances.

Finally, the fluorescence spectrometer sometimes gives inaccurate map results which could be due to technical issues or ambient light interfering with the sample. This was normally tackled by making sure that the sample compartment is properly closed with the lid and repeat the measurement which is time-demanding because each run in the NIR can take up to 1 hour 45 minutes.

Even though I encountered some of these challenges but in general, I really enjoyed this journey because it helps me to understand current experimental techniques for scientific spectral characterization of materials by absorption, photoluminescence excitation and emission mapping. The project also shows how spectroscopy science is helping to identify materials to characterize material interactions in various environments, and to design new compounds.

5 Conclusion

In this dissertation, experiments conducted in the visible and near-infrared range are geared towards understanding energy transfer in the system of SWCNT-surfactant-dye and for characterizing SWCNTs using photoluminescence spectroscopy.

The first primary objective was to do a literature review on SWCNTs functionalization, energy transfer, and photoluminescence imaging as a chapter was carried out and completed transforming lately into Chapter 2 (Background).

The second primary objective was to perform experimental work for mixtures of SWCNT with bis-astraphloxin. The journey started by going through some training on experimental measurements of absorption and photoluminescence spectra, including excitation-emission photoluminescence maps. Followed by samples preparation: neat dispersion of SWCNT, neat solution of the dye, and mixtures of the SWCNT with bis-astraphloxin and then by conducting immediate measurements of absorption and photoluminescence spectra for the samples. The absorption and photoluminescence spectra for mixtures of SWCNT with bis-astraphloxin have been measured. Besides, as a reference, the spectra for the mixture of SWCNT with astraphloxin have also been recorded.

The final primary objective is focused on investigation of the physical mechanism for the energy transfer in the SWCNT-dye system via measured spectral data. It was shown that SWCNT interacts with bis-astraphloxin as the spectra of the mixtures are not a superposition of the spectra of each component: SWCNT or bis-astraphloxin dye only. In the studied mixtures of SWCNT with bis-astraphloxin, it was observed a strong quenching of visible range dye emission and significant enhancement (up to a factor of 4) of the NIR emission of SWCNT in the range of the dye excitation. Plotting the PL intensity vs the emission wavelength for corresponding to a mixture of CNT with astraphloxin of concentration of 0.004 mg/mL and to neat CNTs of various chiralities – (6,5), (7,5) and (8,4), the highest (up to a factor of 6) PL amplification achieved for the (7,5) chirality. This is evidencing efficient energy transfer from the interacting bis-astraphloxin (donor), to SWCNT (acceptor). Comparison of the above mixture with the mixture of astraphloxin-SWCNT and relating to literature data [2], it is possible to associate the interaction and energy transfer due to the formation of ionic complexes of bis-astraphloxin-SWCNT. The complexes are self-assembled due to Coulomb attraction of positively charged bis-astraphloxin and positively charged SWCNT covered by negatively charged surfactant.

The extended objective explored by experimenting and analysing of temporal developments of energy transfer/aggregation in the SWCNT-dye mixtures. Delayed measurements of absorption and photoluminescence spectra for the samples are carried out for updated physical mechanism for the SWCNT-dye energy transfer. It was found that neat solutions of the dye remained stable for weeks

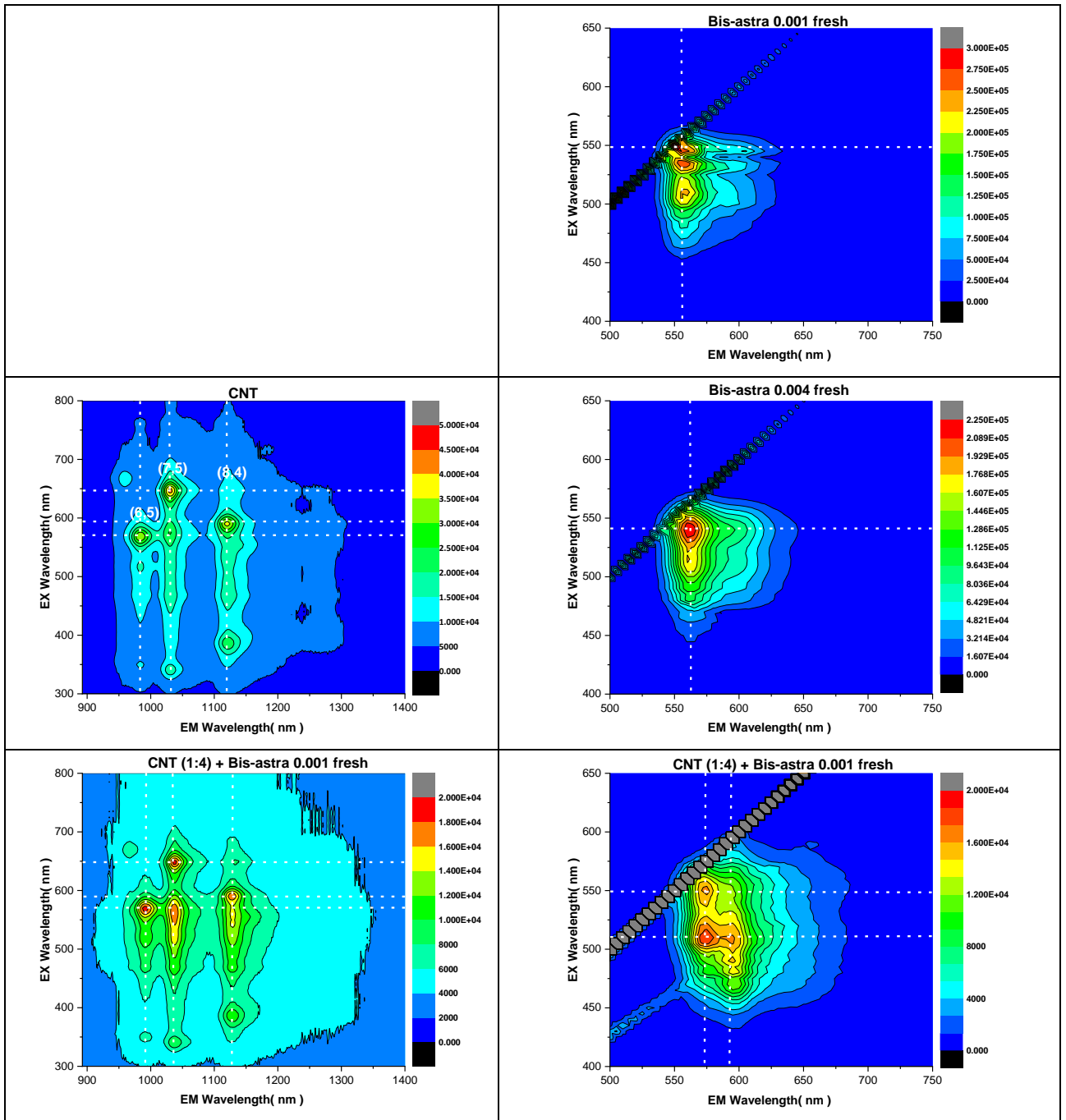
with no aggregation formation. The temporal studies show that energy transfer complexes bis-astrophloxin-SWCNT are formed immediately, however their properties were slightly changing (over a week) depending on the concentration of the dye in the mixture. At low concentration of dye (0.001g/L), the energy transfer peaks of photoluminescence were growing, and for high concentrations (0.008g/L) the energy transfer peaks of emission had a bit lower intensity.

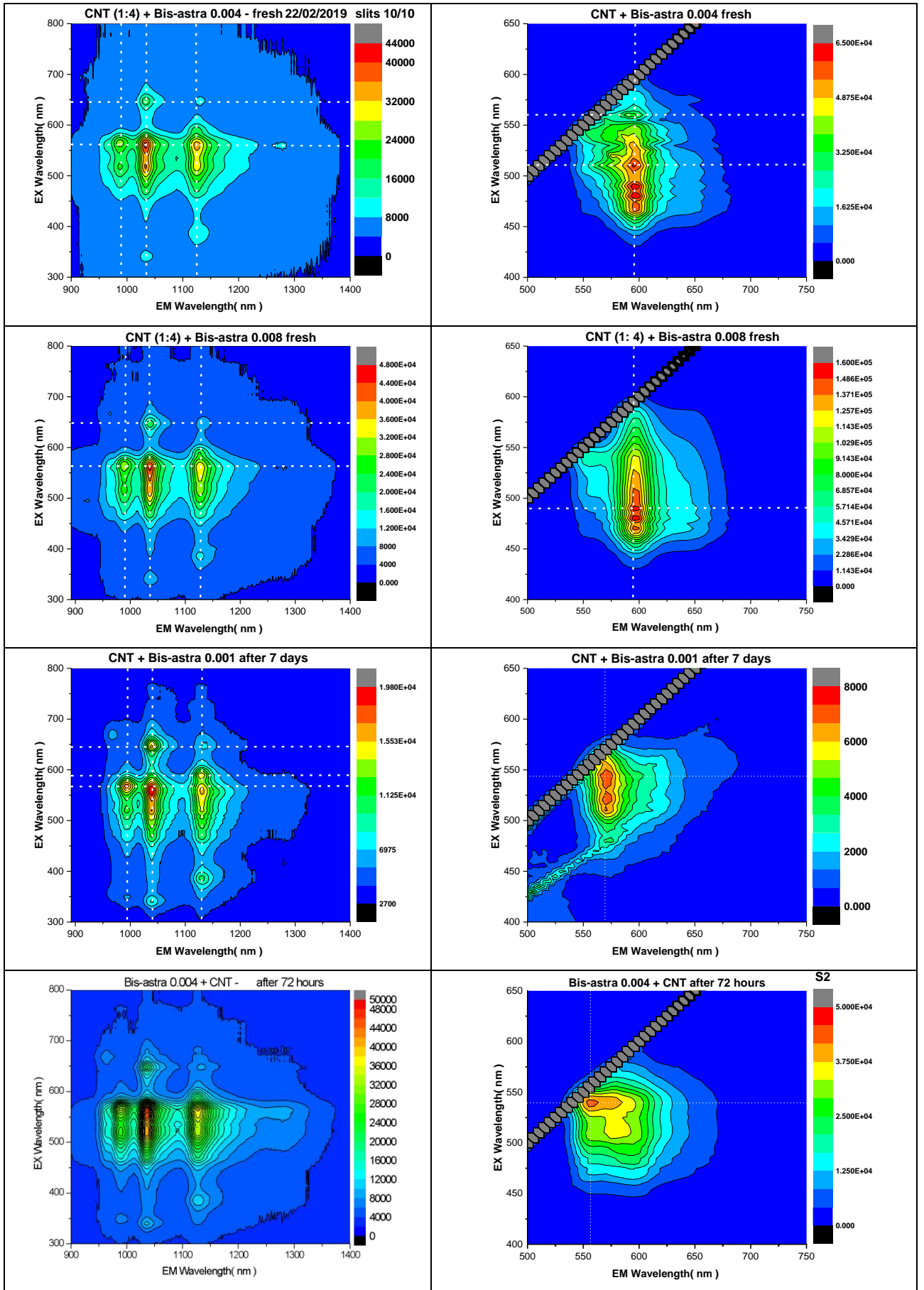
6 REFERENCES

- [1] A. Jain, A. Homayoun, C. Bannister and K. Yum, "Single-walled carbon nanotubes as near-infrared optical biosensors for life sciences and biomedicine," *Biotechnology Journal*, vol. 10, no. 3, pp. 447-459, 2015.
- [2] P. Lutsyk, R. Arif, J. Hruby, A. Bukivskiy, O. Viniychuk, M. Shandura, V. Yakubovskiy, Y. Kovtun, G. Rance, M. Fay, Y. Piryatinski, O. Kachkovsky, A. Verbitsky and A. Rozhin, "A sensing mechanism for the detection of carbon nanotubes using selective photoluminescent probes based on ionic complexes with organic dyes," *Light: Science & Applications*, vol. 5, no. 2, pp. e16028-e16028, 2016.
- [3] K. Kostarelos, A. Bianco and M. Prato, "Promises, facts, and challenges for carbon nanotubes in imaging and therapeutics," 2018.
- [4] A. Hirsch, "The era of carbon allotropes," *Nature Materials*, vol. 9, no. 11, pp. 868-871, 2010. Available: 10.1038/nmat2885.
- [5] "The Periodic Table and Periodic Trends," *2012books.lardbucket.org*, 2019. [Online]. Available: <https://2012books.lardbucket.org/books/principles-of-general-chemistry-v1.0/s11-the-periodic-table-and-periodi.html>. [Accessed: 11- Feb- 2019].
- [6] "All about Pyrophoric Carbon and Longterm Low-temperature - *www.kidskunst.info*," *Kidskunst.info*, 2019. [Online]. Available: <http://www.kidskunst.info/linked/pyrophoric-carbon-and-longterm-lowtemperature-7079726f70686f726963.htm>. [Accessed: 11- Feb- 2019].
- [7] D. Guldi and N. Martín, *Carbon nanotubes and related structures*. Weinheim: Wiley-VCH, 2010.
- [8] *Worldscientific.com*, 2019. [Online]. Available: https://www.worldscientific.com/doi/abs/10.1142/9789814327824_0016. [Accessed: 11- Feb- 2019].
- [9] "A Study of Catalyst Preparation Methods for Synthesis of Carbon Nanotubes," *Chemical Science Transactions*, 2016. Available: 10.7598/cst2016.1109.
- [10] K. Sapsford, L. Berti and I. Medintz, "Materials for Fluorescence Resonance Energy Transfer Analysis: Beyond Traditional Donor-Acceptor Combinations," *Angewandte Chemie International Edition*, vol. 45, no. 28, pp. 4562-4589, 2006. Available: 10.1002/anie.200503873.
- [11] *Arxiv.org*, 2019. [Online]. Available: <https://arxiv.org/ftp/arxiv/papers/1409/1409.5096.pdf>. [Accessed: 04- May- 2019].

- [12] "Photoluminescence", *En.wikipedia.org*, 2019. [Online]. Available: <https://en.wikipedia.org/wiki/Photoluminescence>. [Accessed: 06- May- 2019].
- [13] "Ultraviolet-Visible (UV-Vis) Spectroscopy | Protocol", *Jove.com*, 2019. [Online]. Available: <https://www.jove.com/science-education/10204/ultraviolet-visible-uv-vis-spectroscopy>. [Accessed: 04- May- 2019].
- [14] K. Boom, F. Stein, S. Ernst and K. Morgenstern, "Coverage-Induced Conformational Selectivity", *The Journal of Physical Chemistry C*, vol. 121, no. 37, pp. 20254-20258, 2017. Available: 10.1021/acs.jpcc.7b04986.
- [15] P. Lutsyk, Y. P. Piryatinski, O. D. Kachkovsky, A. Verbitsky, A. G. Rozhin. Unsymmetrical relaxation paths of the excited states in cyanine dyes detected by time-resolved fluorescence: polymethinic and polyenic forms. *Journal of Physical Chemistry A*, vol. 121, 2017, pp. 8236-8246. Available: 10.1021/acs.jpca.7b08680.
- [16] P. Lutsyk, Yu. Piryatinski, M. AlAraimi, R. Arif, M. Shandura, O. Kachkovsky, A. Verbitsky, A. Rozhin. Emergence of additional visible range photoluminescence due to aggregation of cyanine dye - astraphloxin on carbon nanotubes dispersed with anionic surfactant. *Journal of Physical Chemistry C* 120, 2016, pp. 20378-20386. Available: 10.1021/acs.jpcc.6b06272.
- [17] M.P. Shandura, Yu.P. Kovtun, V.P. Yakubovskiy, Yu.P. Piryatinski, P.M. Lutsyk, R.J. Perminov, R.N. Arif, A.B. Verbitsky, A. Rozhin. Dioxaborine dyes as fluorescent probes for amines and carbon nanotubes. *Sensor Letters* vol. 12, 2014, pp. 1361-1367.
- [18] M. Al Araimi, P. Lutsyk, A. Verbitsky, Yu. Piryatinski, M. Shandura, A. Rozhin. A dioxaborine cyanine dye as a photoluminescence probe for sensing carbon nanotubes. *Beilstein Journal of Nanotechnology* vol. 7, 2016, pp.1991–1999.

7 Appendix- MAPS





Functionalization of single-walled carbon nanotubes with bis-astraphloxin

